NASA Contractor Report 194910

ICASE Report No. 94-31

ICASE

EFFECT OF PRESSURE GRADIENT ON FIRST MODE OF INSTABILITY IN HIGH-SPEED BOUNDARY LAYERS

Jamal A. Masad
Yousef H. Zurigat

Contract NAS1-19480
April 1994

Institute for Computer Applications in Science and Engineering
NASA Langley Research Center
Hampton, VA 23681-0001

Operated by Universities Space Research Association

ICASE Fluid Mechanics

Due to increasing research being conducted at ICASE in the field of fluid mechanics, future ICASE reports in this area of research will be printed with a green cover. Applied and numerical mathematics reports will have the familiar blue cover, while computer science reports will have yellow covers. In all other aspects the reports will remain the same; in particular, they will continue to be submitted to the appropriate journals or conferences for formal publication.

Effect of Pressure Gradient on First Mode of Instability in High-Speed Boundary Layers

Jamal A. Masad
High Technology Corporation
Hampton, VA 23666

and

Yousef H. Zurigat[1]
Mechanical Engineering Department
University of Jordan
Amman, Jordan

ABSTRACT

The effect of a pressure gradient on the first mode of instability of compressible subsonic and supersonic boundary layers is investigated using linear stability theory. Formulations are presented for nonsimilar boundary-layer mean flow and linear quasi-parallel stability problems that account for variable fluid properties. A pressure gradient is studied that generates potential-flow Mach number distributions at the edge of the boundary layer of the form $M_e = cx^n$, where c is a constant and x is the dimensionless streamwise distance. Variations are calculated for the maximum growth rates of three-dimensional first-mode waves with different edge Mach numbers and different levels of both adverse and favorable pressure gradients. A favorable pressure gradient is shown to have a stabilizing effect on first-mode waves. However, at high edge Mach numbers, a favorable pressure gradient becomes less effective in stabilizing first-mode waves. The frequencies and streamwise and spanwise wave numbers that correspond to the maximum growth rates of first-mode waves decrease as the pressure gradient becomes more favorable at all Mach numbers when the Reynolds number R = 1500 and at $M_e \geq 2$ when R = 600. Setting the Prandtl number to unity significantly increases the maximum growth rates of first- and second-mode waves at high Mach numbers compared with setting it to the realistic value of 0.72.

[1] This research was supported by the National Aeronautics and Space Administration under NASA Contract No. NAS1-19480 while the second author was in residence at the Institute for Computer Applications in Science and Engineering (ICASE), NASA Langley Research Center, Hampton, VA 23681. The first author's research was supported by NASA Langley Research Center, Hampton, VA, under contract NAS1-19299.

I. INTRODUCTION

Previous experimental and theoretical studies have shown that an adverse pressure gradient destabilizes a laminar boundary layer, whereas a favorable pressure gradient stabilizes it. These effects should be understood and their variations quantified with the large parameter space. Furthermore, the relations between a pressure gradient, stability, and transition make quantifying the effect of a pressure gradient on the stability of boundary layers significant for predicting and controlling transition. In this work, we study the effects of favorable and adverse pressure gradients on the stability of compressible subsonic and supersonic two-dimensional (2-D) boundary layers. The emphasis is on evaluating these effects on first-mode instability.

The effect of a pressure gradient on the stability of three-dimensional (3-D) flows is different from its effect on 2-D flows. The presence of a pressure gradient with a body sweep is a necessary condition to induce crossflow and, therefore, crossflow instability that contributes to the transition to turbulence. Although modern airplane designs use swept wings that induce 3-D flows, the effect of the pressure gradient on the stability of 2-D flows remains important. For example, near the wing box, little crossflow is present and the flow is mostly 2-D. In addition, the flow at the fuselages and nacelles at low angles of attack is axisymmetric with little crossflow.

Theoretical studies of the effect of a pressure gradient on the stability of 2-D incompressible flows have considered both self-similar (Falkner-Skan) and nonsimilar boundary layers. These studies showed that favorable pressure gradients are stabilizing and adverse pressure gradients are destabilizing, which has been confirmed by numerous experimental investigations. The higher modes of instability[1] in high Mach number, compressible flows makes the stability of these flows more complicated than that of low-speed flows.

A favorable pressure gradient in compressible boundary layers is associated with compression and, therefore, with an increase in the Mach number at the edge M_e of the boundary layer. Furthermore, a favorable pressure gradient is also associated with a convex body. However an adverse pressure gradient is associated with expansion, a decrease in M_e and a concave body. The concavity might enhance the growth of Görtler vortices and, consequently, their possible interaction with the T-S waves.

For compressible flow, only a few published studies examine the effect of a pressure gradient on laminar boundary-layer stability. The most recent studies have concentrated on the second-mode instability of boundary layers with a pressure gradient. Malik[2] showed that a favorable pressure gradient stabilizes the second-mode waves by reducing the peak amplification rate and decreasing the band of frequencies that are amplified while the band shifts to higher values. Some of Malik's results were derived from viscous stability analysis of compressible self-similar boundary layers with favorable pressure gradients. As Malik indicated,[2] self-similar solutions in compressible boundary layers with a pressure gradient are not known to exist unless the Prandtl number Pr is set equal to

unity. If Pr is set equal to unity in air boundary layers, the stability characteristics of the flow might change significantly in comparison with setting Pr equal to the realistic value of 0.72. This issue is discussed further in section IV. Malik's stability results with self-similar boundary layers were computed at $M_e = 4.5$ and a Reynolds number $R = 1500$. Malik also performed calculations for a nonsimilar boundary layer that developed on the wall of a hypersonic nozzle with a suction slot ahead of the throat. For that case, the flow accelerates from $M_e = 0.34$ at the lip of the suction slot to $M_e = 6$ toward the exit of the nozzle. Malik performed a stability analysis at two nozzle stations corresponding to $M_e = 4.57$ and $R = 3165$ and to $M_e = 5.45$ and $R = 3648$. In both cases, a favorable pressure gradient was found to reduce the maximum growth rate of second-mode waves and shift the band of unstable frequencies toward higher values.

The effect of an adverse pressure gradient on second-mode instability in flow past a flare cone configuration at a free-stream Mach number $M_\infty = 8$ was studied by Malik et al.[3] The flare cone configurations were designed to produce almost constant streamwise pressure gradients. The mean flow was computed with both parabolized Navier-Stokes and boundary-layer methods and the resulting profiles were analyzed with linear stability theory. The amplification rate of the second-mode disturbances was found to increase with the adverse pressure gradient.

Zurigat et al.[4] showed that second-mode waves are stabilized by favorable pressure gradients and become destabilized by adverse pressure gradients. These results agree with those of Malik.[2] The peak amplification rate for favorable pressure gradients was found to shift toward a higher frequency, which also agrees with the conclusions of Malik[2] at $M_e = 4.5$, 4.57, and 5.45. However, for flow at $M_e = 6.5$, the study of Zurigat et al.[4] showed that the peak amplification rate shifts toward a lower frequency when a favorable pressure gradient is applied.

Vignau[5] (as reported in Arnal et al.[6]) analyzed the effect of adverse pressure gradients for an M_e that varies linearly with x. He considered flows with $M_e = 5$, 5.8, and 7. Vignau found that adverse pressure gradients destabilize second-mode waves and that highly adverse pressure gradients destabilize the usually stable third-mode waves (in zero pressure-gradient flow at finite Reynolds numbers). The experimental study of Kimmel[7] for flow past a fore cone over a flared or an ogive aft body showed that at $M_e = 8$, favorable pressure gradients delayed transition and adverse pressure gradients promoted transition. At $M_e = 8$ the instability was dominated by second-mode waves.

In a zero pressure-gradient, adiabatic compressible boundary layer, when M_∞ exceeds a certain value, the 2-D first- and second-mode waves merge while they are amplified. Zurigat et al.[4] found that both favorable and adverse pressure gradients have very little effect on the growth rates in the merging region. This result indicates that at high Mach numbers, a very strong favorable pressure gradient is necessary to divide the single unstable region in the growth-rate frequency domain into two separate regions.

The study of Vignau[5] reported that first-mode waves are stabilized by adverse pressure gradients. This result is discussed in section IV. Zurigat et al.[4] considered the effect of pressure gradient on 2-D and 3-D first-mode waves at a single spanwise wave number and at the single value of M_e = 2. The flow and disturbance conditions considered by Zurigat et al. do not correspond to the most amplified waves. The present study considers the effect of pressure gradient on first-mode waves under the most amplified conditions. We point out here that, although the most unstable second-mode waves are 2-D, the most unstable first-mode waves in supersonic boundary layers are 3-D.[1]

II. FORMULATION

We consider the Navier-Stokes equations describing a 3-D, unsteady, compressible perfect gas flowing over a surface. We choose a body-oriented orthogonal coordinate system with the axes x^*, y^*, and z^* such that x^* is measured from the attachment line along the surface, y^* is measured from the surface in the normal direction, and z^* extends in the spanwise direction such that the coordinate system is right handed. We assume that no body forces exist and that no heat is added (from within the flow or from radiation). The dimensional Navier-Stokes equations describing this flow are the continuity, momentum, energy, and state equations

$$\frac{\partial \rho^*}{\partial t^*} + \vec{\nabla}^* \cdot \left(\rho^* \vec{V}^*\right) = 0 \tag{1}$$

$$\rho^* \left(\frac{\partial \vec{V}^*}{\partial t^*} + \vec{V}^* \cdot \vec{\nabla}^* \vec{V}^* \right) = -\vec{\nabla}^* p^* + \vec{\nabla}^* \cdot \vec{\vec{\tau}}^* \tag{2}$$

$$\rho^* \frac{Dh^*}{Dt^*} = \frac{Dp^*}{Dt^*} + \left(\kappa^* T_{,i}^*\right)_{,i} + \Phi^* \tag{3}$$

$$p^* = \rho^* R^* T^* \tag{4}$$

where

$$\tau_{ij}^* = \lambda^* e_{kk}^* \delta_{ij} + 2\mu^* e_{ij}^* \tag{5a}$$

$$\Phi^* = \lambda^* \left(e_{ii}^*\right)^2 + 2\mu^* e_{ij}^* e_{ij}^* \tag{5b}$$

$$e_{ij}^* = \frac{1}{2}\left(\frac{\partial v_i^*}{\partial x_j^*} + \frac{\partial v_j^*}{\partial x_i^*} \right) \tag{5c}$$

$$\vec{\nabla}^* = \vec{i} \frac{\partial}{\partial x^*} + \vec{j} \frac{\partial}{\partial y^*} + \vec{k} \frac{\partial}{\partial z^*} \tag{5d}$$

$$\vec{V}^* = \vec{i}\,u^* + \vec{j}v^* + \vec{k}w^* \tag{5e}$$

In the above equations, τ_{ij}^* is the stress tensor, e_{ij}^* the rate of strain tensor, Φ^* is the dissipation function, and δ_{ij} is the Kronecker delta. Furthermore, the indices in the index notation have the values 1, 2, and 3 and $v_1^* = u^*$, $v_2^* = v^*$, $v_3^* = w^*$, $x_1^* = x^*$, $x_2^* = y^*$, and $x_3^* = z^*$. In equation (3) D/Dt, is the material derivation given (for any quantity s^*) by

$$\frac{Ds^*}{Dt^*} = \frac{\partial s^*}{\partial t^*} + \vec{V}^* \cdot \vec{\nabla}^* s^* \tag{6}$$

and in the index notation

$$s_{,_i}^* = \frac{\partial s^*}{\partial x_i} \tag{7}$$

for any quantity s^*. In the above equations, ρ^* is the density, t^* is time, $\vec{V}^*$ is the velocity vector with its components u^*, v^*, and w^* in the x^*, y^*, and z^* directions, respectively. The pressure is p^*, the enthalpy is h^*, the thermal conductivity is κ^*, the absolute temperature is T^*, the dynamic viscosity is μ^*, the second coefficient of viscosity is λ^*, and the universal gas constant is R^*. The unit vectors $\vec{i}$, $\vec{j}$, and $\vec{k}$ are in the x^*, y^*, and z^* directions, respectively.

For a perfect gas,

$$h^* = \int C_p^* dT^* \tag{8}$$

We render the Navier-Stokes equations nondimensional by defining

$$(x, y, z) = \frac{(x^*, y^*, z^*)}{L^*} \tag{9a}$$

$$t = \frac{t^* U_r^*}{L^*} \tag{9b}$$

$$\vec{V} = \frac{\vec{V}^*}{U_r^*} \tag{9c}$$

$$\rho = \frac{\rho^*}{\rho_r^*} \tag{9d}$$

$$p = \frac{p^*}{\rho_r^* U_r^{*2}} \tag{9e}$$

$$(\lambda, \mu) = \frac{(\lambda^*, \mu^*)}{\mu_r^*} \tag{9f}$$

$$\kappa = \frac{\kappa^*}{\kappa_r^*} \tag{9g}$$

$$C_p = \frac{C_p^*}{C_{p,r}^*} \tag{9h}$$

$$T = \frac{T^*}{T_r^*} \tag{9i}$$

where L^* is a reference length and the subscript r denotes a reference quantity. Using and expanding equations (8)–(9i) in equations (1)–(4), we get

$$\frac{\partial \rho}{\partial t} + \frac{\partial}{\partial x}(\rho u) + \frac{\partial}{\partial y}(\rho v) + \frac{\partial}{\partial z}(\rho w) = 0 \tag{10}$$

$$\rho\left(\frac{\partial u}{\partial t} + u\frac{\partial u}{\partial x} + v\frac{\partial u}{\partial y} + w\frac{\partial u}{\partial z}\right) = -\frac{\partial p}{\partial x} + \frac{1}{Re_r}\left\{\frac{\partial}{\partial x}\left[(\lambda + 2\mu)\frac{\partial u}{\partial x} + \lambda\left(\frac{\partial v}{\partial y} + \frac{\partial w}{\partial z}\right)\right] + \frac{\partial}{\partial y}\left[\mu\left(\frac{\partial u}{\partial y} + \frac{\partial v}{\partial x}\right)\right]\right.$$

$$\left. + \frac{\partial}{\partial z}\left[\mu\left(\frac{\partial u}{\partial z} + \frac{\partial w}{\partial x}\right)\right]\right\} \tag{11}$$

$$\rho\left(\frac{\partial v}{\partial t} + u\frac{\partial v}{\partial x} + v\frac{\partial v}{\partial y} + w\frac{\partial v}{\partial z}\right) = -\frac{\partial p}{\partial y} + \frac{1}{Re_r}\left\{\frac{\partial}{\partial x}\left[\mu\left(\frac{\partial \mu}{\partial y} + \frac{\partial v}{\partial x}\right)\right]\right.$$

$$\left. + \frac{\partial}{\partial y}\left[(\lambda + 2\mu)\frac{\partial v}{\partial y} + \lambda\left(\frac{\partial u}{\partial x} + \frac{\partial w}{\partial z}\right)\right] + \frac{\partial}{\partial z}\left[\mu\left(\frac{\partial v}{\partial z} + \frac{\partial w}{\partial y}\right)\right]\right\} \tag{12}$$

$$\rho\left(\frac{\partial w}{\partial t} + u\frac{\partial w}{\partial x} + v\frac{\partial w}{\partial y} + w\frac{\partial w}{\partial z}\right) = -\frac{\partial p}{\partial z} + \frac{1}{Re_r}\left\{\frac{\partial}{\partial x}\left[\mu\left(\frac{\partial u}{\partial z} + \frac{\partial w}{\partial x}\right)\right]\right.$$

$$\left. + \frac{\partial}{\partial y}\left[\mu\left(\frac{\partial v}{\partial z} + \frac{\partial w}{\partial y}\right)\right] + \frac{\partial}{\partial z}\left[(\lambda + 2\mu)\frac{\partial w}{\partial z} + \lambda\left(\frac{\partial u}{\partial x} + \frac{\partial v}{\partial y}\right)\right]\right\} \tag{13}$$

$$\rho\left(C_p\frac{\partial T}{\partial t} + C_p u\frac{\partial T}{\partial x} + C_p v\frac{\partial T}{\partial y} + C_p w\frac{\partial T}{\partial z}\right) = (\gamma - 1)M_r^2\left[\frac{\partial p}{\partial t} + u\frac{\partial p}{\partial x} + v\frac{\partial p}{\partial y} + w\frac{\partial p}{\partial z} + \frac{1}{Re_r}\Phi\right]$$

$$+ \frac{1}{Re_r Pr_r}\left[\frac{\partial}{\partial x}\left(\kappa\frac{\partial T}{\partial x}\right) + \frac{\partial}{\partial y}\left(\kappa\frac{\partial T}{\partial y}\right) + \frac{\partial}{\partial z}\left(\kappa\frac{\partial T}{\partial z}\right)\right] \tag{14}$$

$$p = \rho\bar{R}_r T \tag{15}$$

where

$$\Phi = (\lambda + 2\mu)\left[\left(\frac{\partial u}{\partial x}\right)^2 + \left(\frac{\partial v}{\partial y}\right)^2 + \left(\frac{\partial w}{\partial z}\right)^2\right] + 2\lambda\left[\frac{\partial u}{\partial x}\frac{\partial v}{\partial y} + \frac{\partial u}{\partial x}\frac{\partial w}{\partial z} + \frac{\partial v}{\partial y}\frac{\partial w}{\partial z}\right]$$

$$+\mu\left[\left(\frac{\partial u}{\partial y}\right)^2 + \left(\frac{\partial u}{\partial z}\right)^2 + \left(\frac{\partial v}{\partial x}\right)^2 + \left(\frac{\partial v}{\partial z}\right)^2 + \left(\frac{\partial w}{\partial x}\right)^2 + \left(\frac{\partial w}{\partial y}\right)^2\right] + 2\mu\left[\frac{\partial u}{\partial y}\frac{\partial v}{\partial x} + \frac{\partial u}{\partial z}\frac{\partial w}{\partial x} + \frac{\partial v}{\partial z}\frac{\partial w}{\partial y}\right] \tag{16}$$

$$Re_r = \frac{U_r^* L_r^* \rho_r^*}{\mu_r^*} \tag{17a}$$

$$(\gamma - 1)M_r^2 = \frac{U_r^{*2}}{C_{p,r}^* T_r^*} \tag{17b}$$

$$Pr_r = \frac{\mu_r^* C_{p,r}^*}{\kappa_r^*} \tag{17c}$$

and

$$\overline{R}_r = \frac{R^* T_r^*}{U_r^{*2}} \tag{17d}$$

We can identify Re_r, M_r, and Pr_r based on the reference quantities. In equation (17b), $\gamma = C_p / C_v$ is the ratio of specific heats, which is assumed to be constant.

A. Mean Flow

We consider 2-D steady flow over a body extending infinitely in the spanwise direction. The body can be curved; therefore, it could exhibit a pressure gradient. However, the flow is perpendicular to the body at the attachment line (no sweep, spanwise velocity $w = 0$); therefore, the flow is 2-D. It follows that

$$\frac{\partial}{\partial t} = 0, \quad \frac{\partial}{\partial z} = 0, \quad w = 0 \tag{18}$$

Our interest here is in boundary-layer flows. To derive the boundary-layer equations for the flow we are considering, we let

$$y = \frac{\overline{y}}{\sqrt{Re_r}} \tag{19a}$$

$$v = \frac{\overline{v}}{\sqrt{Re_r}} \tag{19b}$$

Furthermore, we take the reference quantities as those at the free stream ∞ and replace the subscript r with ∞. Substituting equations (18)–(19b) into equations (10)–(15) and assuming $Re_r = Re_\infty$ is large, we obtain, to the leading order,

$$\frac{\partial}{\partial x}(\rho u)+\frac{\partial}{\partial \bar{y}}(\rho \bar{v})=0 \tag{20}$$

$$\rho\left(u\frac{\partial u}{\partial x}+\bar{v}\frac{\partial u}{\partial \bar{y}}\right)=-\frac{\partial p}{\partial x}+\frac{\partial}{\partial \bar{y}}\left(\mu\frac{\partial u}{\partial \bar{y}}\right) \tag{21}$$

$$\frac{\partial p}{\partial \bar{y}}=0 \tag{22}$$

$$\rho C_p\left(u\frac{\partial T}{\partial x}+\bar{v}\frac{\partial T}{\partial \bar{y}}\right)=(\gamma-1)M_\infty^2\left[u\frac{\partial p}{\partial x}+\mu\left(\frac{\partial u}{\partial \bar{y}}\right)^2+\frac{1}{Pr_\infty}\frac{\partial}{\partial \bar{y}}\left(\kappa\frac{\partial T}{\partial \bar{y}}\right)\right] \tag{23}$$

and

$$p=\rho\bar{R}_\infty T \tag{24}$$

The boundary conditions at the wall are

$$u=0 \quad \text{at} \quad \bar{y}=0 \tag{25}$$

$$\bar{v}=\sqrt{Re_\infty}v_w=\sqrt{Re_\infty}\frac{v_w^*}{U_\infty^*} \quad \text{at} \quad \bar{y}=0 \tag{26}$$

and

$$\left.\begin{array}{ll} & \dfrac{\partial T}{\partial \bar{y}}=0 \\ \text{or} & \\ & T=T_w=\dfrac{T_w^*}{T_\infty^*} \end{array}\right\} \quad \text{at} \quad \bar{y}=0 \tag{27}$$

Equation (25) is the no-slip condition. In equation (26), v_w^* is the suction ($v_w^* < 0$) or blowing ($v_w^* > 0$) velocity at the wall and for an impermeable wall $\bar{v}=v_w^*=0$. The first condition in equation (27) is for an adiabatic surface, whereas the second is for some specified distribution of the wall absolute temperature T_w^*. At a large $\bar{y}$ we have

$$u \to u_e \quad \text{as} \quad \bar{y} \to \infty \tag{28}$$

$$T \to T_e \quad \text{as} \quad \bar{y} \to \infty \tag{29}$$

where u_e and T_e are the nondimensional streamwise velocity and temperature at the edge of the boundary layer, respectively. They are made nondimensional with respect to U_∞^* and T_∞^* and, thus,

$$u_e = \frac{u_e^*}{U_\infty^*} \tag{30a}$$

$$T_e = \frac{T_e^*}{T_\infty^*} \tag{30b}$$

It follows from expression (22) that

$$p = p(x) \tag{31}$$

If equation (24) is applied the edge of the boundary layer, then we get

$$p_e = \rho_e \overline{R}_\infty T_e \tag{32}$$

At the same $x, p = p_e$; therefore,

$$\rho T = \rho_e T_e \tag{33}$$

To transform the boundary-layer equations using the Levy-Lees variables, we let

$$\xi(x) = \int_0^x \rho_e \mu_e u_e dx \tag{34a}$$

$$\eta(x, \bar{y}) = \frac{u_e}{\sqrt{2\xi}} \int_0^{\bar{y}} \rho d\bar{y} \tag{34b}$$

$$F = \frac{u}{u_e} \tag{34c}$$

$$Q = \frac{T}{T_e} \tag{34d}$$

$$V = \frac{\sqrt{2\xi}}{\rho_e \mu_e u_e}\left[\rho\bar{v} + \eta_x \sqrt{2\xi} F\right] \tag{34e}$$

$$\beta_0 = \frac{2\xi}{u_e}\frac{du_e}{d\xi} \tag{34f}$$

and

$$\theta = \frac{\rho\mu}{\rho_e \mu_e} \tag{34g}$$

With equations (33) and (34), we can show that equations (20)–(24) transform into

$$2\xi F_\xi + V_\eta + F = 0 \tag{35}$$

$$2\xi F F_\xi + V F_\eta - \left(\theta F_\eta\right)_\eta + \beta_0\left(F^2 - Q\right) = 0 \tag{36}$$

$$2\xi F Q_\xi + \frac{2\xi}{T_e}\frac{dT_e}{d\xi} F Q\left(1 - \frac{C_{p,e}}{C_p}\right) + V Q_\eta - \frac{1}{C_p}\left(\frac{\theta C_p}{Pr} Q_\eta\right)_\eta - (\gamma - 1) M_\infty^2 \frac{u_e^2}{C_p T_e} \theta F_\eta^2 = 0 \tag{37}$$

To reach equation (36), we used the relation

$$\frac{dp}{dx} = -\rho_e u_e \frac{du_e}{dx} \tag{38}$$

which follows from applying equation (21) at the edge of the boundary layer.

The boundary conditions in expressions (25)–(29) transform into

$$F = 0 \quad \text{at} \quad \eta = 0 \tag{39}$$

$$V = \frac{\sqrt{2\xi}}{\rho_e \mu_e u_e} \rho \sqrt{Re_\infty}\, \frac{v_w^*}{U_\infty^*} \quad \text{at} \quad \eta = 0 \tag{40}$$

$$\left.\begin{array}{l} Q_\eta = 0 \\ \text{or} \\ Q = Q_w = \dfrac{T_w}{T_e} \end{array}\right\} \quad \text{at} \quad \eta = 0 \tag{41}$$

$$F \to 1, \quad Q \to 1 \quad \text{as} \quad \eta \to \infty \tag{42}$$

The variations of the fluid properties with temperature are given in appendix A. The potential flow quantities and their relation to the free-stream quantities are given in appendix B.

For a constant C_p and a constant Pr, $C_{p,e} = C_p = 1$ and, therefore, equations (35)–(37) reduce to the familiar form

$$2\xi F_\xi + V_\eta + F = 0 \tag{43}$$

$$2\xi F F_\xi + V F_\eta - \left(\theta F_\eta\right)_\eta + \beta_0\left(F^2 - Q\right) = 0 \tag{44}$$

$$2\xi F Q_\xi + V Q_\eta - \frac{1}{Pr}\left(\theta Q_\eta\right)_\eta - (\gamma - 1) M_\infty^2 \frac{u_e^2}{T_e} \theta F_\eta^2 = 0 \tag{45}$$

The boundary conditions corresponding to those given by equations (39)–(42) do not change with a constant C_p and Pr.

To study the effect of pressure gradients on the stability of compressible boundary layers, we could select a certain body with a surface that exhibits a pressure gradient, solve the mean-flow problem over the surface, and study the stability of the resulting profiles. The second option is to specify some streamwise variation of the potential flow velocity u_e or the potential flow M_e. In the study of Zurigat et al.,[4] as well as in this work, the pressure gradient is assumed to correspond to a boundary-layer edge Mach number distribution of the form

$$M_e = cx^n$$

where c is a constant and x is the dimensionless streamwise distance.

B. Stability

We consider the linear quasi-parallel stability of the mean flow described in the previous section III.A in relation to 3-D unsteady disturbances. Stability studies that account for the nonparallel effects[8–14] in compressible flow over a flat plate showed that these effects can be significant within certain ranges of the parameter space. The effect of nonparallelism on the stability of 2-D compressible flow with a pressure gradient is unknown; therefore, the results presented in this work using the quasi-parallel assumption should be interpreted accordingly. Furthermore, the effect of the body curvature on the stability of 2-D high-speed flows is unknown. Preliminary calculations performed by Malik (private communications, 1993) indicate that this effect can be significant for certain parameters. However, this effect is not accounted for in the present study. The stability analysis accounts for variable fluid properties; such a formulation with these properties was introduced earlier,[15,9,14] and we present it here for completeness. To perform the analysis, we scale the Navier-Stokes equations and make them nondimensional by defining

$$(x,y,z) = \frac{\left(x^*,y^*,z^*\right)}{\delta_r^*} \tag{46a}$$

$$t = \frac{t^* U_e^*}{\delta_r^*} \tag{46b}$$

$$\vec{V} = \frac{\vec{V}^*}{u_e^*} \tag{46c}$$

$$\rho = \frac{\rho^*}{\rho_e^*} \tag{46d}$$

$$p = \frac{p^*}{\rho_e^* u_e^{*2}} \tag{46e}$$

$$(\lambda,\mu)=\frac{(\lambda^*,\mu^*)}{\mu_e^*} \tag{46f}$$

$$\kappa=\frac{\kappa^*}{\kappa_e^*} \tag{46g}$$

$$C_p=\frac{C_p^*}{C_{p,e}^*} \tag{46h}$$

and

$$T=\frac{T^*}{T_e^*} \tag{46i}$$

where

$$\delta_r^*=\sqrt{\frac{\nu_e^* x^*}{u_e^*}} \tag{47}$$

We use equations (46a)–(46i) in equations (1)–(4) and assume each dependent quantity as a superposition of a mean quantity and a disturbance quantity; thus, we let

$$(u,v,w)=(u_m,v_m,0)+(\tilde{u},\tilde{v},\tilde{w}) \tag{48a}$$

$$\rho=\rho_m+\tilde{\rho} \tag{48b}$$

$$p=p_m+\tilde{p} \tag{48c}$$

$$T=T_m+\tilde{T} \tag{48d}$$

$$(\mu,\lambda)=(\mu_m,\lambda_m)+(\tilde{\mu},\tilde{\lambda}) \tag{48e}$$

$$\kappa=\kappa_m+\tilde{\kappa} \tag{48f}$$

and

$$C_p=C_{p,m}+\tilde{C}_p \tag{48g}$$

If we use equations (48a)–(48g) in the scaled nondimensional Navier-Stokes equations, subtract the basic state, linearize and impose the quasi-parallel assumption, then we obtain the following disturbance equations (after suppressing the tilde for convenience):

$$\frac{\partial\rho}{\partial t}+\rho_m\frac{\partial u}{\partial x}+u_m\frac{\partial\rho}{\partial x}+\rho_m\frac{\partial v}{\partial y}+\frac{d\rho_m}{dy}v+\rho_m\frac{\partial w}{\partial z}=0\ , \tag{49}$$

$$\rho_m\left(\frac{\partial u}{\partial t}+u_m\frac{\partial u}{\partial x}+\frac{du_m}{dy}v\right)=-\frac{\partial p}{\partial x}+\frac{1}{R}\left\{\mu_m\frac{\partial}{\partial x}\left(r\frac{\partial u}{\partial x}+m\frac{\partial v}{\partial y}+m\frac{\partial w}{\partial z}\right)\right.$$

$$\left.+\frac{\partial}{\partial y}\left[\mu_m\left(\frac{\partial u}{\partial y}+\frac{\partial v}{\partial x}\right)+\mu\frac{du_m}{dy}\right]+\mu_m\frac{\partial}{\partial z}\left(\frac{\partial u}{\partial z}+\frac{\partial w}{\partial z}\right)\right\}, \tag{50}$$

$$\rho_m\left(\frac{\partial v}{\partial t}+u_m\frac{\partial v}{\partial x}\right)=-\frac{\partial p}{\partial y}+\frac{1}{R}\left\{\mu_m\frac{\partial}{\partial x}\left(\frac{\partial u}{\partial y}+\frac{\partial v}{\partial x}\right)+\frac{du_m}{dy}\frac{\partial \mu}{\partial x}\right.$$

$$\left.+\frac{\partial}{\partial y}\left[\mu_m\left(r\frac{\partial v}{\partial y}+m\frac{\partial u}{\partial x}+m\frac{\partial w}{\partial z}\right)\right]+\mu_m\frac{\partial}{\partial z}\left(\frac{\partial v}{\partial z}+\frac{\partial w}{\partial y}\right)\right\}, \tag{51}$$

$$\rho_m\left(\frac{\partial w}{\partial t}+u_m\frac{\partial w}{\partial x}\right)=-\frac{\partial p}{\partial z}+\frac{1}{R}\left\{\mu_m\frac{\partial}{\partial x}\left(\frac{\partial u}{\partial z}+\frac{\partial w}{\partial x}\right)\right.$$

$$\left.+\frac{\partial}{\partial y}\left[\mu_m\left(\frac{\partial v}{\partial z}+\frac{\partial w}{\partial y}\right)\right]+\mu_m\frac{\partial}{\partial z}\left(r\frac{\partial w}{\partial z}+m\frac{\partial u}{\partial x}+m\frac{\partial v}{\partial y}\right)\right\} \tag{52}$$

and

$$\rho_m C_p\left(\frac{\partial T}{\partial t}+u_m\frac{\partial T}{\partial x}+\frac{dT_m}{dy}v\right)=(\gamma_e-1)M_e^2\left[\frac{\partial p}{\partial t}+u_m\frac{\partial p}{\partial x}+\frac{1}{R}\phi\right]$$

$$+\frac{1}{RPr_e}\left[\kappa_m\frac{\partial^2 T}{\partial x^2}+\frac{\partial}{\partial y}\left(\kappa_m\frac{\partial T}{\partial y}+\kappa\frac{dT_m}{dy}\right)+\kappa_m\frac{\partial^2 T}{\partial z^2}\right] \tag{53}$$

where

$$\phi=2\mu_m\left(\frac{du_m}{dy}\frac{\partial u}{\partial y}+\frac{du_m}{dy}\frac{\partial v}{\partial x}\right)+\mu\left(\frac{du_m}{dy}\right)^2 \tag{54}$$

The disturbance equation of state is

$$\frac{p}{p_m}=\frac{T}{T_m}+\frac{\rho}{\rho_m}, \tag{55}$$

where

$$r=2+\frac{\lambda_m}{\mu_m}, \tag{56a}$$

$$m=\frac{\lambda_m}{\mu_m}, \tag{56b}$$

$$R=\frac{u_e^*\delta_r^*}{\nu_e^*} \tag{56c}$$

and

$$C_p = C_{p,m} \tag{56d}$$

Because μ and κ are functions of temperature only, we have

$$\mu = \frac{d\mu_m}{dT_m} T \tag{57a}$$

$$\kappa = \frac{d\kappa_m}{dT_m} T \tag{57b}$$

We seek solutions for equations (49)–(55) in the form

$$[u, v, p, T, w] = [\zeta_1(y), \zeta_3(y), \zeta_4(y), \zeta_5(y), \zeta_7(y)] \exp\left[i\left(\int \alpha \, dx + \beta z - \omega t \right) \right] . \tag{58}$$

If we substitute equation (58) into equations (49)–(55), we obtain

$$D\zeta_3 + i\alpha\zeta_1 - \frac{DT_m}{T_m}\zeta_3 + i(\alpha u_m - \omega)\left(\gamma_e M_e^2 \zeta_4 - \frac{\zeta_5}{T_m} \right) + i\beta\zeta_7 = 0 , \tag{59}$$

$$i(\alpha u_m - \omega)\zeta_1 + \zeta_3 Du_m + i\alpha T_m \zeta_4 - \frac{T_m}{R}\left[-\mu_m\left(r\alpha^2 + \beta^2\right)\zeta_1 - \alpha\beta\mu_m(m+1)\zeta_7 + i(m+1)\alpha\mu_m D\zeta_3 \right.$$

$$\left. + DT_m\mu_m' D\zeta_1 + i\alpha DT_m\mu_m'\zeta_3 + \mu_m D^2\zeta_1 + D\left(\mu_m' Du_m\right)\zeta_5 + \mu_m' Du_m\zeta_5 \right] = 0 , \tag{60}$$

$$i(\alpha u_m - \omega)\zeta_3 + T_m D\zeta_4 - \frac{T_m}{R}\left[i(m+1)\alpha\mu_m D\zeta_1 + im\alpha DT_m\mu_m'\zeta_1 - \left(\alpha^2 + \beta^2\right)\mu_m\xi_3 \right.$$

$$\left. + rDT_m\mu_m' D\zeta_3 + im\beta DT_m\mu_m'\zeta_7 + i\alpha\mu_m' Du_m\zeta_5 + r\mu_m D^2\zeta_3 + i(m+1)\beta\mu_m D\zeta_7 \right] = 0 , \tag{61}$$

$$i(\alpha u_m - \omega)\zeta_7 + i\beta T_m\zeta_4 - \frac{T_m}{R}\left[-(m-1)\alpha\beta\mu_m\zeta_1 + i\beta DT_m\mu_m'\zeta_3 + i\mu_m(m+1)\beta D\zeta_3 \right.$$

$$\left. - \mu_m\left(\alpha^2 + r\beta^2\right)\zeta_7 + DT_m\mu_m' D\zeta_7 + \mu_m D^2\zeta_7 \right] = 0 \tag{62}$$

and

$$iC_p(\alpha u_m - \omega)\zeta_5 + DT_m C_p\zeta_3 - i(\gamma_e - 1)M_e^2 T_m(\alpha u_m - \omega)\zeta_4$$

$$- \frac{(\gamma_e - 1)M_e^2 T_m}{R}\left[2Du_m\mu_m(D\zeta_1 + i\alpha\zeta_3) + \mu_m'(Du_m)^2\zeta_5 \right]$$

$$- \frac{T_m}{RPr_e}\left[-\kappa_m\left(\alpha^2 + \beta^2\right)\zeta_5 + \kappa_m D^2\zeta_5 + 2\kappa_m' D\zeta_5 D\zeta_5 + \kappa_m' D^2 T_m\zeta_5 + \left(DT_m\right)^2\kappa_m''\zeta_5 \right] = 0 , \tag{63}$$

where the prime indicates differentiation with respect to T_m and $D = \partial / \partial y$.

Equations (59)–(63) can be cast into the following set of eight coupled first-order ordinary differential equations:

$$D\zeta_n - \sum_{m=1}^{8} f_{nm}\zeta_m = 0, \quad n = 1,2,...,8, \tag{64}$$

where $\zeta_2 = D\zeta_1$, $\zeta_6 = D\zeta_5$, and $\zeta_8 = D\zeta_7$ and the nonzero coefficients f_{nm} are defined in appendix C. The boundary conditions are

$$\zeta_1 = \zeta_3 = \zeta_5 = \zeta_7 = 0 \quad \text{at } y = 0 \tag{65}$$

and

$$\zeta_n \quad \text{is bounded as} \quad y \to \infty \tag{66}$$

The corresponding equations for constant C_p and Pr are obtained by setting

$$C_p = C_{p,m} = 1$$

and

$$\gamma_e = \gamma = \text{constant}$$

in the coefficients in appendix C. The resulting equations are found in many references (e.g., Zurigat et al.[4])

III. METHODS OF SOLUTION

The nonsimilar boundary-layer mean-flow equations with pressure gradient are solved with an initial zero pressure-gradient region of length x_0 to avoid the singularity at $x = 0$. At $x = x_0$ (< 1), the flow starts to undergo compression or expansion at a rate determined by the choice of n in the equation $M_e = cx^n$. Positive values of n produce favorable pressure gradients; negative values of n produce adverse pressure gradients. This compression or expansion terminates at $x = 1$; M_e reaches a desired value M_d that is set a priori. The free-stream Mach number is chosen such that $M_e = M_d$ when ($x = 1$). Stability calculations are carried out at $x = 1$, which allows a comparison to be made between favorable and adverse pressure gradient results at the same edge Mach number and stability Reynolds number.

Equations (43)–(45) and the boundary conditions in equations (39)–(42) are solved with a finite-difference method and a Newton-Raphson linearization. The discretization and solution procedure follow those described by Blottner.[16] The special case of self-similar boundary layers is obtained by dropping the leading terms in equations (43)–(45). This self-similar solution is then used to start its nonsimilar counterpart. The dependence of the value of the pressure gradient parameter β_0 on the length of the initial zero pressure-gradient region x_0 is very weak. For example, at $M_\infty = 4.5$ and

$n = -0.2$, a change of x_0 from 0.2 to 0.05 increases the value of β_0 by only 0.3 percent. However, a switch from a zero pressure gradient to a nonzero pressure gradient flow region corresponds to a sudden change in the geometry of the surface and could introduce an upstream effect on the mean flow; the parabolic nonsimilar boundary-layer theory does not account for this effect.

The stability problem is solved by a second-order-accurate finite-difference scheme with deferred correction[17] coupled with a Newton–Raphson iteration on the eigenvalue. More details of the method are given by Asfar et al.[18]

IV. RESULTS

A. Mean Flow

Variations of M_e with the streamwise distance are shown in Figure 1 for several values of n. As was discussed in the previous section, the length of the initial region in which the pressure gradient is assumed to be zero has a very small effect on the mean flow calculations at $x = 1$. The streamwise velocity and the temperature profiles at $x = 1$ with the same parameters shown in Figure 1 are shown in Figures 2(a) and 2(b), respectively. Figure 2(a) clearly shows that a favorable pressure gradient changes the streamwise velocity profile by making it fuller, which stabilizes the flow.

The zero pressure-gradient compressible flow has a single generalized inflection point inside the boundary layer; a favorable pressure gradient creates another generalized inflection point near the wall (Fig. 3). The generalized inflection point is defined as the point where $D(\rho_m Du_m) = 0$ with $D = \partial/\partial y$, u_m is the streamwise mean-flow velocity component, and ρ_m is the mean-flow density. The significance of a generalized inflection point at $y = y_s$ inside the boundary layer, where $y_s > y_o$ at which $u_m(y_o) = 1 - M_e^{-1}$, is that it makes the boundary layer unstable to inviscid disturbances. The generalized inflection point can be thought of as the compressible analog of the inflection point in incompressible flows, which is responsible for making the flow inviscidly unstable. As the favorable pressure gradient level increases, the two generalized inflection points move closer until they meet and disappear (Fig. 3). Figure 3 clearly demonstrates that the minimum favorable pressure gradient level needed to eliminate the generalized inflection points increases as M_e increases.

B. Stability

The quantities R, F, and B will be used to present the stability results. The Reynolds number R is given by equation (56c). The frequency f^* is the dimensional frequency of the disturbance in cycles per second (hertz), and it remains constant for the same physical wave. The dimensional circular frequency ω^* is given by

$$\omega^* = 2\pi f^* \tag{67}$$

and the nondimensional circular frequency ω is defined as

$$\omega = \omega^* \delta_r^* / u_e^* \tag{68}$$

where δ_r^* is defined in equation (47). The frequency parameter F is defined as

$$F = \omega / R \tag{69}$$

and equations (67)–(69) and equation (56c) show that

$$F = \frac{2\pi f^* \nu_e^*}{u_e^{*2}} \tag{70}$$

The dimensional spanwise wave number is β^*, which remains constant for the same physical wave. The nondimensional spanwise wave number β is defined as

$$\beta = \beta^* \delta_r^* \tag{71}$$

We also define a nondimensional spanwise wave number parameter B as

$$\beta = 1000\beta / R \tag{72}$$

Equations (71), (72), and (56c) lead to

$$B = \frac{1000\beta^* \nu_e^*}{u_e^*} \tag{73}$$

Furthermore, Re_x is defined as

$$Re_x = \frac{u_e^* x^*}{\nu_e^*}$$

or

$$Re_x = \left(\frac{u_e^*}{\nu_e^*}\right) \frac{u_e^*}{\nu_e^*} \delta_r^{*2}$$

or

$$Re_x = R^2 \tag{74}$$

We start by presenting stability results that demonstrate the importance of the first mode in the transition process. To this end, the predicted transition location in compressible flow over a flat plate was calculated from the empirical e^9 method. A wave with a fixed dimensional frequency and a fixed dimensional spanwise wave number was followed as it propagated downstream. The Reynolds number where the N factor reached 9 ($(\mathrm{Re}_x)_{N=9}$) was determined. The dimensional frequency and

spanwise wave number were varied to compute the lowest $(\mathrm{Re}_x)_{N=9}$. Variation of the predicted transition Reynolds number with the free-stream Mach number when transition is due to first- or second-mode waves is shown in Figure 4. The figure clearly shows that the e^9 method predicts that transition is due to first-mode waves up to M_∞ = 6 to 6.5. Results similar to those shown in Figure 4 for flow past a cone with zero and small pressure gradients were computed and presented by Lysenko.[19] The computations were performed by solution of the Dunn-Lin[20] stability equations and the results show that the predicted transition is due to first-mode waves up to M ≈ 7.

To study the effects of favorable and adverse pressure gradients on the first mode of instability in compressible boundary layers, we considered flows with a pressure gradient parameter n = 0.1, 0, and –0.1 and a potential flow M_e that ranges from 0 to the hypersonic value of 7.4. The variation of the maximum growth rate of first-mode waves with M_e was computed for all three values of n. The results are shown in Figure 5(a). The growth rates were maximized over both the frequency and the spanwise wave number. The step in F was chosen to be 0.1×10^{-6}, and the step in the spanwise wave number β was chosen to be 0.001. The stabilizing effect of a favorable pressure gradient on the first mode of instability and at all values M_e is very clear in Figure 5(a). The effectiveness of a favorable pressure gradient in reducing the maximum growth rates of first-mode waves diminishes at high supersonic and hypersonic Mach numbers, which is also evident in Figure 5(a). Note in Figure 5(a) that for zero and adverse pressure gradients, compressibility reduces the maximum growth rate; for the favorable pressure gradient case of n = 0.1, compressibility increases the maximum growth rate. The increase in the maximum growth rate when n = 0.1 results from the ineffective pressure gradient at high values of M_e. A decrease in the effective pressure gradient when the value of the critical Reynolds number changes as the Mach number increases was demonstrated in the asymptotic calculations of Shapiro[21] for 2-D disturbances at M_e = 1.5 to 3. Also shown in figure 5(a) is the variation of the maximum growth rate of second-mode waves at the same R and for the same values of n.

The streamwise wave numbers, frequencies, and spanwise wave numbers that correspond to the maximum growth rates in Figure 5(a) are shown in Figures 5(b) through 5(d), respectively. By increasing M_e, the most amplified spanwise wave number remains at zero (2-D wave) to nearly sonic values, where it increases sharply, reaches a peak, then starts to decrease slowly (Fig. 5(d)). Then it encounters another sharp increase, reaches a second peak, and is followed by a second range of slow decrease. As the pressure gradient becomes more favorable, both peaks shift toward higher values of M_e. Figures 5(b) and 5(c) show that the most amplified frequencies and streamwise wave numbers of first-mode waves decrease as the pressure gradient becomes more favorable. The most amplified spanwise wave numbers decrease for all values of M_e as the pressure gradient becomes more favorable.

Results similar to those shown in Figure 5 but at R = 600 are shown in Figure 6. The values of n are –0.12, –0.06, 0, and 0.06. The general features in Figure 6 at R = 600 are similar to those in Figure 5 at R = 1500. However, the most amplified frequencies and streamwise wave numbers in figure 6 decrease as the pressure gradient becomes more favorable at $M_e \geq 2$, whereas in figure 5 they decrease at all values of M_e, although the decrease in Figure 5 is small at low values of M_e. This performance of the streamwise wave numbers and the frequencies that correspond to the maximum growth rates of first-mode waves at R = 600 are similar to those of second-mode waves (Figs. 5(b) and 5(c)). This result indicates that if we compute and plot the variation of the maximum growth rate (over all spanwise wave numbers) versus the frequency at fixed M_e and at R = 600, then at low values of M_e the peak amplification is expected to decrease and shift toward higher values of F as the pressure gradient becomes more favorable. However, at high values of M_e, the peak amplification is expected to decrease and shift toward lower values of F as the pressure gradient becomes more favorable.

The decrease in the effective favorable pressure gradient on stabilizing the first- and second-mode disturbances at high Mach numbers is disturbing in regard to the natural laminar flow of high-speed flow. This ineffectiveness suggests that other methods should be explored to delay transition and to improve the efficiency of high-speed aerodynamic surfaces.

In the results presented thus far, first-mode waves were found to become destabilized by adverse pressure gradients. These results seem to disagree with the results of Vignau[5] (as reported in Arnal et al.[6]). The results of Vignau show that the critical Reynolds number of first-mode waves increases with adverse pressure gradients. This finding also seems to disagree with the results of the asymptotic calculations of Shapiro[21] for two-dimensional first-mode disturbances. The calculations of Shapiro[22] showed clearly that the critical Reynolds number decreases with an adverse pressure gradient for M_e = 1.5 to 3. However, the details of the work of Vignau[5] are not available in English. Furthermore, the reference length scale in the work of Vignau is the displacement thickness and not δ_r^* (given by equation (47)). We believe that what seems to be a disagreement among the results of Vignau, the present results, and the results of Shapiro is more likely due to the use of different reference length scales in the two sets of results.

Zurigat et al.[4] showed that the variation of the maximum growth rate of 2-D second-mode waves (for the considered flow with $M_e = cx^n$) with n is almost linear. This linear performance was found to break down close to separation. To determine if the linearity persists in the case of first-mode waves, the maximum growth rate of first-mode waves (over all frequencies and spanwise wave numbers) was computed as a function of n for M_e = 0, 2, 4, and 6 at R = 1500. The results are shown in Figure 7, and the variation is clearly almost linear. However, the linearity breaks down close to separation (not shown in the figure), and the maximum growth rate increases significantly. Such linearity can be utilized to compute the maximum growth rate for any n based on the values at two different

values of n and can also be used in the context of an envelope method to correlate transition. The circles in Figure 7 indicate results of calculations in which the length of the initial zero pressure-gradient region is $x_0 = 0.1$, whereas for the rest of the results, $x_0 = 0.2$. Thus, a change in x_0 from 0.2 to 0.1 has virtually no effect on the value of the maximum growth rate.

Next, we considered the transverse distribution of fluctuation amplitude. Computations were made at $M_e = 0$, 2, and 6 for an adverse, zero, and a favorable pressure gradient. The parameters correspond to some points in Figure 7. For $M_e = 0$, only the distribution of streamwise velocity fluctuations is presented, whereas for $M_e = 2$ and 6, the distributions of streamwise velocity and temperature fluctuations are presented. The results for $M_e = 0$, 2, and 6 are shown in Figures 8–10, respectively. In Figure 8 and for $n = 0$, the distribution is standard for 2-D disturbances in incompressible flow over a flat plate, which is characterized by two peaks wherein the peak close to the wall is larger than the peak away from the wall. A favorable pressure gradient shifts the lower peak slightly and the upper peak significantly toward the wall. The adverse pressure gradient with a magnitude close to inducing separation creates the three-peak structure shown in Figure 8. This structure is very similar to that noted theoretically[22,23] and experimentally[24] within a separation bubble caused by a roughness element. The middle peak is believed to be due to shear-layer instability. Note in Figure 8 that as the pressure gradient becomes less adverse or more favorable, the disturbance decays faster in the free stream. The distribution of the phase at $n = -0.1$ (not shown) exhibits two phase jumps similar to those found theoretically[25] and experimentally[24] in a separation bubble caused by a roughness element. For $M_e = 2$, the distributions of the magnitudes of streamwise velocity and temperature fluctuations are shown in Figures 9(a) and 9(b), respectively. For both quantities, the distributions of the adverse pressure gradient are characterized by three peaks, whereas for $n = 0$ and $n = 0.11$, only two peaks are evidenced. The temperature fluctuation distribution in Figure 9(b) at $n = -0.15$ is similar to that found by Masad and Nayfeh[23] for separating flow over a roughness element at $M_\infty = 0.8$. For $M_e = 6$, the distributions of the magnitudes of streamwise velocity and temperature fluctuations are shown in Figures 10(a) and 10(b), respectively. Note that the shifts in the peaks in Figures 8–10 do not necessarily correspond to the shifts of the dimensional physical fluctuation. This situation occurs because y in Figures 8–10 is y^* / δ_r^* and δ_r^* is given by equation (47), which shows clearly that δ_r^* depends on the value of the pressure gradient and Mach number. Therefore, the shifts should be interpreted accordingly.

As mentioned in the introduction, self-similar solutions of compressible boundary layers with a pressure gradient exist only when the Prandtl number is set equal to unity. Furthermore, many investigators use a Prandtl number of unity because it simplifies the mean-flow problems. When the Prandtl number is set to unity and a pressure gradient is present , an analytic expression exists for the temperature profile.[26] This same expression holds when the Prandtl number is unity, the wall is adiabatic, and the pressure gradient is zero.[26] Changing the Prandtl number from 0.72 to 1.0 causes

a relatively small increase in the maximum growth rate at subsonic Mach numbers (Fig. 11); however, it increases the maximum growth rate significantly at high Mach numbers. The significant destabilizing effect of setting the Prandtl number to unity at high Mach numbers is true for both first- and second-mode waves. When the Prandtl number is changed from 0.72 to 1.0, the frequencies and the streamwise and spanwise wave numbers that correspond to the maximum growth rates of the first-mode waves increase, particularly at high Mach numbers.

V. CONCLUSIONS

Linear stability theory is used to study the effect of a pressure gradient on the first mode of instability in compressible subsonic and supersonic boundary layers. Formulations are presented for the nonsimilar boundary-layer mean flow and stability problems that account for variable fluid properties. Consideration is given to the effects of both favorable and adverse pressure gradients on the stability of flows at Mach numbers of 0 to 7.

Although a favorable pressure gradient does have a stabilizing effect on first-mode waves, it becomes less effective in stabilizing these waves at high-edge Mach numbers. Also, both the frequencies and the streamwise and spanwise wave numbers that correspond to the maximum growth rates of first-mode waves decrease as the pressure gradient becomes more favorable at all Mach numbers when the Reynolds number is 1500 and at Mach numbers that are higher than approximately 2 when the Reynolds number is 600. Setting the Prandtl number to unity does increase the maximum growth rates significantly at high Mach numbers.

REFERENCES

1. L. M. Mack, "Boundary-layer stability theory," Jet Propulsion Laboratory Technical Report 90zero 277, Rev. A (1969).

2. M. R. Malik, "Prediction and control of transition in supersonic and hypersonic boundary layers," *AIAA Journal*, **27**, No. 11, 1487 (1989).

3. M. R. Malik, P. Balakumar, and C.-L. Chang, "Effect of adverse pressure gradient on the second mode instability in hypersonic boundary layers," HTC Report HTC-9006, December (1990).

4. Y. H. Zurigat, A. H. Nayfeh and J. A. Masad, "Effect of pressure gradient on the stability of compressible boundary layers," *AIAA Journal*, **30**, No. 9, 2204 (1992).

5. F. Vignau, "Etude theorique et experimentale de la transition en ecoulement bidimensionnel compressible," Thesis, ENSAE, Toulouse (1989).

6. D. Arnal, F. Vignau, and F. Laburthe, "Recent supersonic transition studies with emphasis on the swept cylinder case," *Proceedings of Boundary Layer Transition and Control Conference*, Peterhouse College, Cambridge, UK (1991).

7. R. L. Kimmel, "Experimental transition zone lengths in pressure gradient in hypersonic flow," in *Transitional and Turbulent Compressible Flows*, ed. L. D. Kral and T. A. Zang, **151**, 117 (1993).

8. N. M. El-Hady, "Nonparallel instability of supersonic and hypersonic boundary layers," *Physics of Fluids A*, **3**, No. 9, 2164 (1991).

9. F. P. Bertolotti, "Compressible boundary layer stability analyzed with the PSE equations," AIAA Paper 91-1637 (1991).

10. F. P. Bertolotti and Th. Herbert," Analysis of the linear stability of compressible boundary layers using the PSE," Theoretical and Computational Fluid Dynamics, **3**, 117 (1991).

11. C.-L. Chang, M. R. Malik, G. Erlebacher, and M. Y. Hussaini," Compressible stability of growing boundary layers using parabolized stability equations," AIAA Paper 91-1636 (1991).

12. C.-L. Chang and M. R. Malik," Non-parallel stability of compressible boundary layers," AIAA Paper 93-2912 (1993).

13. S. A. Gapanov, "The influence of flow nonparallelism on disturbances development in supersonic boundary layers," in Proceedings of the Eighth Canadian Congress of Applied Mechanics, 673 (1981).

14. J. A. Masad, A. H. Nayfeh, and A. A. Al-Maaitah, "Effect of heat transfer on the stability of compressible boundary layers," *Computers and Fluids*, **21**, No. 1, 43 (1992).

15. H. L. Reed and P. Balakumar, "Compressible boundary-layer stability theory," *Physics of Fluids A*, **2**, No. 8, 1341 (1990).

16. F. G. Blottner, "Investigation of some finite-difference techniques for solving the boundary layer equations," *Computer Methods in Applied Mechanics and Engineering*, **6**, 1 (1975).

17. V. Pereyra, "PASVA3: An adaptive finite-difference Fortran program for first-order nonlinear ordinary boundary-value problems," *Lect. Notes Comput. Sci.*, **76**, 67 (1976).

18. O. R. Asfar, J. A. Masad, and A. H. Nayfeh, "A method for calculating the stability of boundary layers," *Computers and Fluids*, **18**, No. 3, 305 (1990).

19. V. I. Lysenko, "The role of the first and second modes in compressible boundary-layer transition," *Applied Dynamics*, 809 (1986).

20. C. C. Lin, "The theory of hydrodynamic stability," Cambridge University Press, Cambridge, (1955).

21. N. M. Shapiro, "Effect of pressure gradient and heat transfer on the stability of the compressible laminar boundary layers," *Journal of Aeronautical Sciences*, **23**, 81 (1956).

22. A. H. Nayfeh, S. A. Ragab, and A. A. Al-Maaitah, "Effect of bulges on the stability of boundary layers," *Physics of Fluids*, **31**, 796 (1988).

23. J. A. Masad and A. H. Nayfeh, "Effect of a bulge on the subharmonic instability of subsonic boundary layers," *AIAA Journal*, **30**, No. 7, 1731 (1992).

24. A. V. Dovgal and V. V. Kozlov, "Hydrodynamic instability and receptivity of small scale separation regions," in Laminar-Turbulent Transition, edited by D. Arnal and R. Michel, Springer, Berlin, 523 (1990).

25. J. A. Masad and A. H. Nayfeh, "Stability of separating boundary layers," in Proceedings of the Fourth International Conference of Fluid Mechanics, Alexandria, Egypt, April 28–30, 1992, I, pp. 261–278.

26. H. Schlichting, Boundary-Layer Theory, McGraw-Hill, Seventh Edition (1979).

Appendix A – Variations of Fluid Properties with Temperature

The variations of μ^*, κ^*, and C_p^* with temperature are given by

$$\mu^* = \frac{1.458 T^{*3/2} \times 10^{-5}}{T^* + 110.4}, \qquad \text{for } T^* > 110.4,$$

$$\mu^* = 0.693873 \times 10^{-6} T^*, \qquad \text{for } T^* \le 110.4,$$

$$\kappa^* = \frac{0.6325 T^{*1/2} \times 10^{-5}}{1 + \left(215.4 / T^*\right) \times 10^{-12/T^*}}, \quad \text{for } T^* > 80.0,$$

$$\kappa^* = 0.222964 \times 10^{-6} T^*, \qquad \text{for } T^* \le 80,$$

and

$$C_p^* = 0.0686042 \left(a_0 + a_1 T^* + a_2 T^{*2} + a_3 T^{*3} \right),$$

where $a_0 = 3.657$, $a_1 = -1.272 \times 10^{-3}$, $a_2 = 2.955 \times 10^{-6}$, $a_3 = -1.365 \times 10^{-9}$, all the quantities are in centimeter-gram-second units, and T^* is in degrees Kelvin.

Appendix B – Potential and Free-Stream Flow Relationships

For steady, 2-D inviscid (potential) flow at the edge of the boundary layer, equations (10)–(15) reduce to

$$\frac{\partial}{\partial x}(\rho_e u_e)+\frac{\partial}{\partial y}(\rho_e v_e)=0 \tag{B1}$$

$$\rho_e\left(u_e\frac{\partial u_e}{\partial x}+v_e\frac{\partial u_e}{\partial y}\right)=-\frac{\partial p_e}{\partial x} \tag{B2}$$

$$\rho_e\left(u_e\frac{\partial v_e}{\partial x}+v_e\frac{\partial v_e}{\partial y}\right)=-\frac{\partial p_e}{\partial y} \tag{B3}$$

$$\rho_e\left(C_{p,e}u_e\frac{\partial T_e}{\partial x}+C_{p,e}v_e\frac{\partial T_e}{\partial y}\right)=(\gamma-1)M_\infty^2\left[u_e\frac{\partial p_e}{\partial x}+v_e\frac{\partial p_e}{\partial y}\right] \tag{B4}$$

$$p_e=\rho_e\overline{R}_\infty T_e \tag{B5}$$

where

$$\overline{R}_\infty=\frac{R^*T_\infty^*}{U_\infty^{*2}} \tag{B6}$$

The reference quantities are based on ∞ and e.

By considering the leading order and by ignoring the viscous-inviscid interaction problem, we obtain $v_e=\frac{\partial v_e}{\partial x}=0$ even when suction velocity is present. Therefore, equations (B1)–(B5) become

$$\frac{\partial}{\partial x}(\rho_e u_e)+\rho_e\frac{\partial v_e}{\partial y}=0 \tag{B7}$$

$$\rho_e u_e\frac{\partial u_e}{\partial x}=-\frac{\partial p_e}{\partial x} \tag{B8}$$

$$\frac{\partial p_e}{\partial y}=0 \tag{B9}$$

$$\rho_e C_{p,e}u_e\frac{\partial T_e}{\partial x}=(\gamma-1)M_\infty^2u_e\frac{\partial p_e}{\partial x} \tag{B10}$$

and

$$p_e=\rho_e\overline{R}_\infty T_e \tag{B5}$$

where

$$\overline{R}_\infty=\frac{R^*T_\infty^*}{U_\infty^{*2}} \tag{B6}$$

If equation (B8) in equation (B10) are used, then we obtain

$$\int_0^x C_{p,e} dT_e = -(\gamma - 1) M_\infty^2 \frac{u_e^2}{2} + C_1$$

at $x = 0$ and $u_e = u_e^* / U_\infty^* = 1$, therefore,

$$\int_0^x C_{p,e} dT_e = \frac{(\gamma - 1) M_\infty^*}{2} \left(1 - u_e^2\right) \tag{B11}$$

for a constant C_p, $C_{p,e} = 1$, then,

$$T_e = 1 + \frac{\gamma - 1}{2} M_\infty^2 \left(1 - u_e^2\right) \qquad \text{constant } C_p \tag{B12}$$

Equation (B5) shows us that

$$\frac{dp_e}{dx} = \overline{R}_\infty \frac{d}{dx}(\rho_e T_e)$$

Using equation (B8) in the above equation yields

$$\overline{R}_\infty \frac{d}{dx}(\rho_e T_e) = -\rho_e u_e \frac{du_e}{dx}$$

However, equation (B12) shows for constant C_p that

$$\frac{dT_e}{dx} = -(\gamma - 1) M_\infty^2 u_e \frac{du_e}{dx} \qquad \text{constant } C_p$$

The above two equations demonstrate that

$$(\gamma - 1) M_\infty^2 \overline{R}_\infty \left(\rho_e \frac{dT_e}{dx} + T_e \frac{d\rho_e}{dx}\right) = \rho_e \frac{dT_e}{dx} \qquad \text{constant } C_p$$

However, for a constant C_p, we have

$$(\gamma - 1) M_\infty^2 \overline{R}_\infty = \frac{U_\infty^{*2}}{T_\infty^* C_p^*} \frac{R^* T_\infty^*}{U_\infty^{*2}} = \frac{\gamma - 1}{\gamma}$$

Then,

$$(\gamma - 1) T_e \frac{d\rho_e}{dx} = \rho_e \frac{dT_e}{dx}$$

Appendix C

Coefficients for equation (64)

The nonzero elements are

$$f_{12} = f_{56} = f_{78} = 1 ,$$

$$f_{21} = \alpha^2 + \beta^2 - i\hat{\omega}R/\mu_m T_m ,$$

$$f_{22} = -D\mu_m/\mu_m ,$$

$$f_{23} = -i\alpha(m+1)DT_m/T_m - i\alpha D\mu_m/\mu_m + RDu_m/\mu_m T_m ,$$

$$f_{24} = i\alpha R/\mu_m + (m+1)\gamma_e M_e^2 \alpha\hat{\omega} ,$$

$$f_{25} = -\alpha(m+1)\hat{\omega}/T_m - D(\mu_m' Du_m)/\mu_m ,$$

$$f_{26} = -\mu_m' Du_m/\mu_m ,$$

$$f_{31} = -i\alpha ,$$

$$f_{33} = DT_m/T_m ,$$

$$f_{34} = i\gamma_e M_e^2 \hat{\omega} ,$$

$$f_{35} = -i\hat{\omega}/T_m ,$$

$$f_{37} = -i\beta ,$$

$$f_{41} = -i\chi\alpha(rDT_m/T_m + 2D\mu_m/\mu_m) ,$$

$$f_{42} = -i\chi\alpha ,$$

$$f_{43} = \chi\left[-\alpha^2 - \beta^2 + i\hat{\omega}R/\mu_m T_m + rD^2 T_m/T_m + rD\mu_m DT_m/\mu_m T_m\right] ,$$

$$f_{44} = -i\chi r\gamma_e M_e^2\left[\alpha Du_m - \hat{\omega}DT_m/T_m - \hat{\omega}D\mu_m/\mu_m\right] ,$$

$$f_{45} = i\chi\left[r\alpha Du_m/T_m + \mu_m'\alpha Du_m/\mu_m - r\hat{\omega}D\mu_m/\mu_m T_m\right] ,$$

$$f_{46} = -i\chi r\hat{\omega}/T_m ,$$

$$f_{47} = -i\chi r\beta DT_m/T_m - 2i\chi\beta D\mu_m/\mu_m ,$$

$$f_{48} = -i\chi\beta ,$$

$$f_{62} = -2(\gamma_e - 1)M_e^2 \,\mathrm{Pr}_e\, Du_m\mu_m/\kappa_m ,$$

$$f_{63} = R\,\mathrm{Pr}_e\,DT_m C_p / T_m \kappa_m - 2i\alpha(\gamma_e - 1)M_e^2\,\mathrm{Pr}_e\,Du_m \mu_m / \kappa_m \ ,$$

$$f_{64} = -i(\gamma_e - 1)M_e^2 R\,\mathrm{Pr}_e(\alpha u_m - \omega)/\kappa_m \ ,$$

$$f_{65} = iR\,\mathrm{Pr}_e\,C_p(\alpha u_m - \omega)/T_m \kappa_m - (\gamma_e - 1)M_e^2\,\mathrm{Pr}_e\,\mu_m'(Du_m)^2/\kappa_m + \alpha^2 + \beta^2 - \kappa_m' D^2 T_m/\kappa_m - \kappa_m'(DT_m)^2/\kappa_m \ ,$$

$$f_{66} = -2\kappa_m' DT_m/\kappa_m \ ,$$

$$f_{83} = -i(m+1)\beta DT_m/T_m - i\beta D\mu_m/\mu_m \ ,$$

$$f_{84} = (m+1)\gamma_e M_e^2 \beta\hat{\omega} + i\beta R/\mu_m \ ,$$

$$f_{85} = -(m+1)\beta\hat{\omega}/T_m \ ,$$

$$f_{87} = \alpha^2 + \beta^2 - i\hat{\omega}R/\mu_m T_m$$

and

$$f_{88} = -D\mu_m/\mu_m \ ,$$

where

$$\mu_m' = d\mu_m/dT_m, \quad DF = \partial F/\partial y, \quad \hat{\omega} = \omega - \alpha u_m, \quad \chi = \left[R/\mu_m - ir\gamma_e M_e^2\hat{\omega}\right]^{-1}, \quad r = 2 + \frac{\lambda_m}{\mu_m}, \quad m = \frac{\lambda_m}{\mu_m} \ .$$

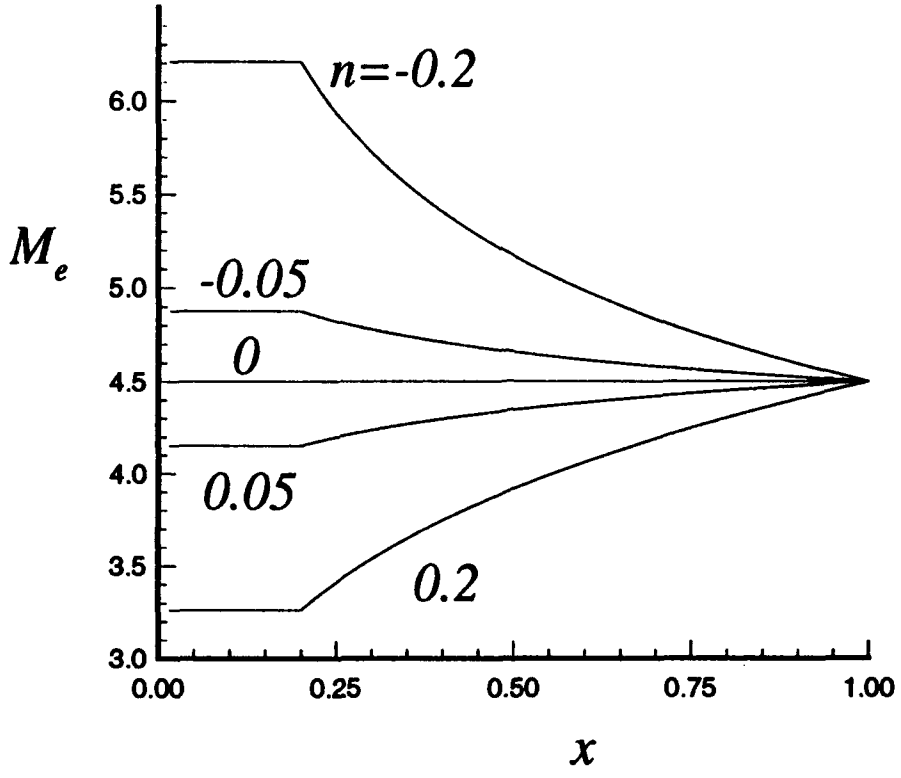

Figure 1. Boundary-layer edge Mach number distributions for different degrees of compression and expansion that terminate at $M_e = 4.5$, $T_\infty = 120$ K, and $Pr = 0.72$.

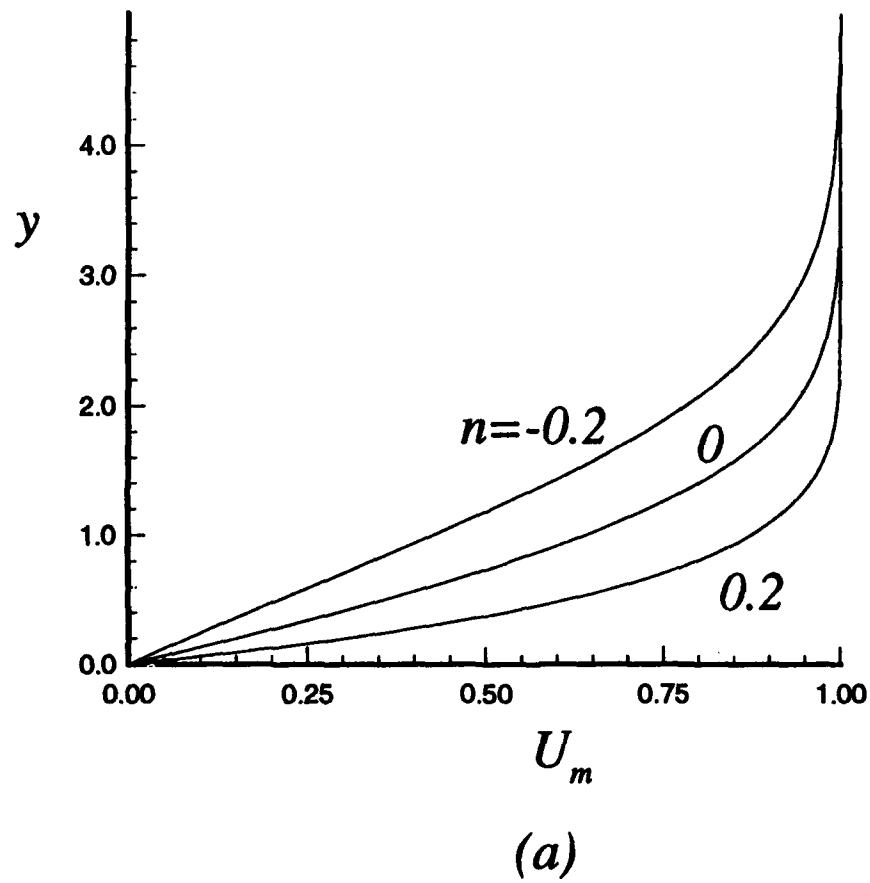

Figure 2. Boundary-layer (a) velocity and (b) temperature distributions for different pressure-gradient parameters $M_e = 4.5$ at $x = 1$, $T_\infty = 120$ K, and $Pr = 0.72$.

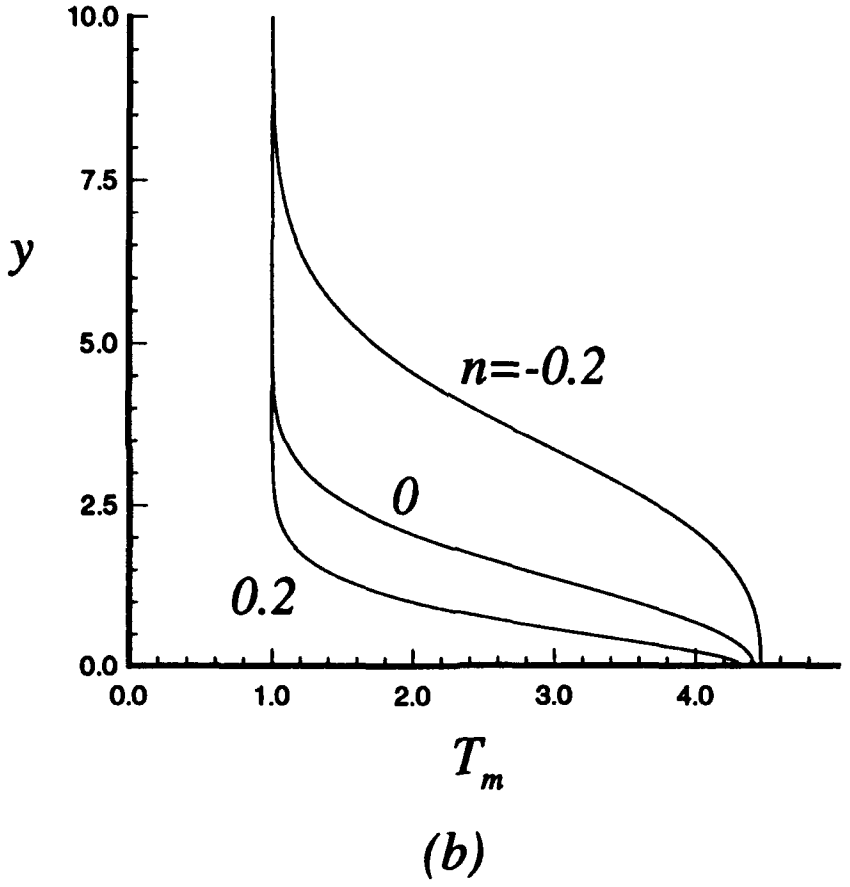

(b)

Figure 2. Concluded.

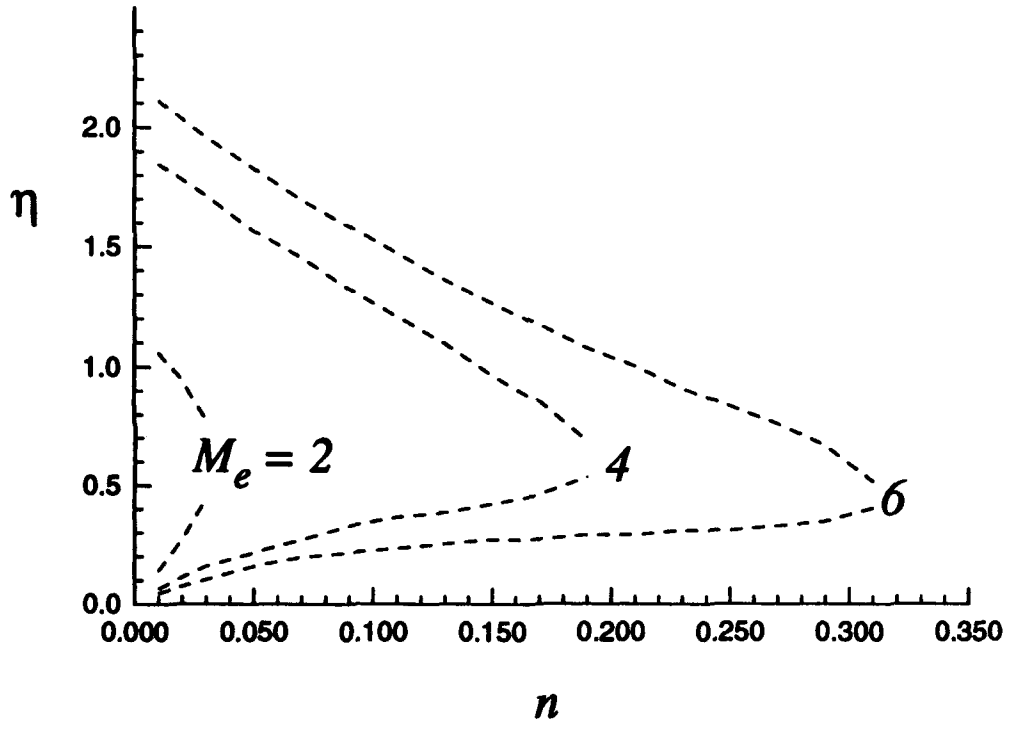

Figure 3. Transverse variation of location of generalized inflection points with pressure-gradient parameter at T_∞ = 120 K and Pr = 0.72.

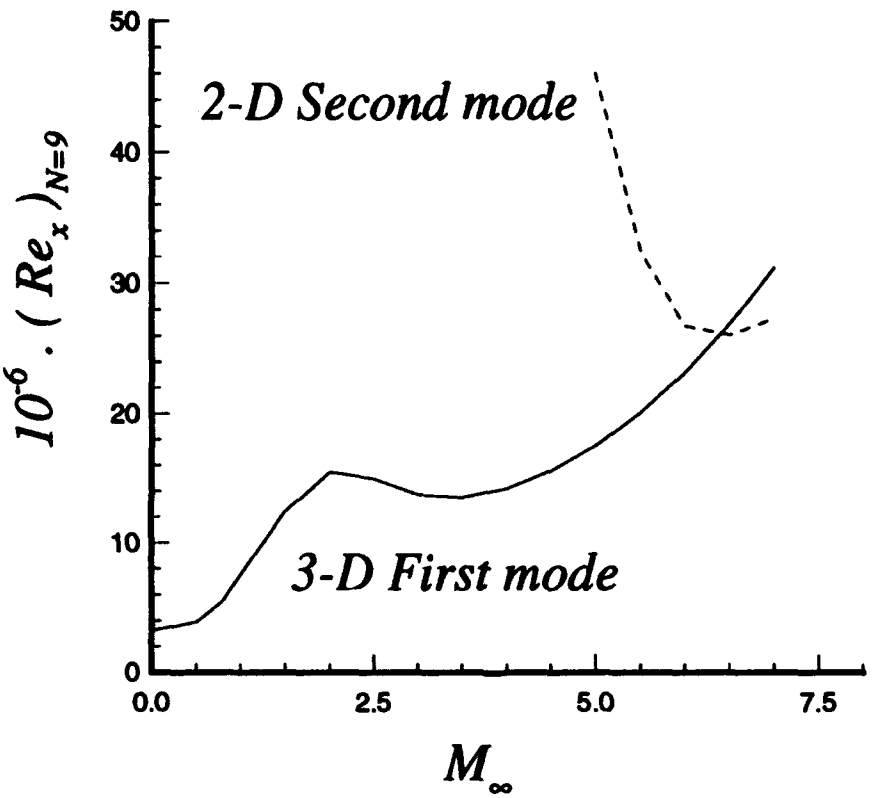

Figure 4. Variation of predicted transition Reynolds number using e^9 method with free-stream Mach number for flow over a flat plate at T_∞ = 150 K and Pr = 0.72.

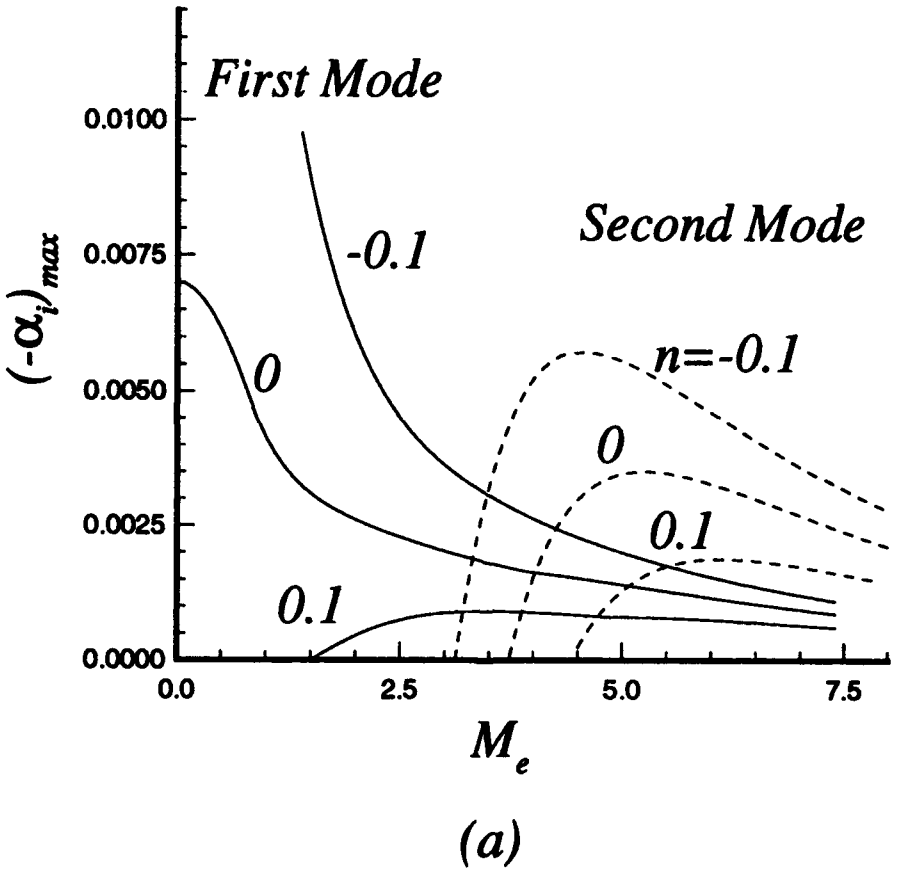

Figure 5. (a) Variation of maximum growth rate with edge Mach number for three levels of pressure gradient at R = 1500, Pr = 0.72, and T_∞ = 120 K; (b) Corresponding streamwise wave numbers; (c) Corresponding frequencies; and (d) Corresponding spanwise wave-number parameters.

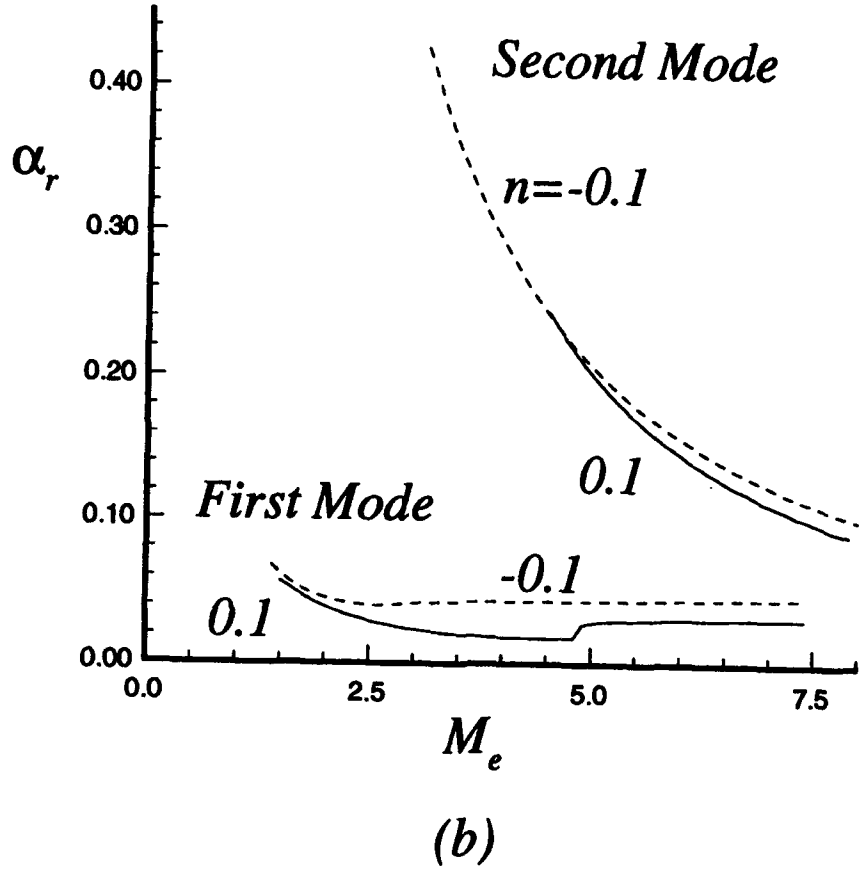

Figure 5. Continued.

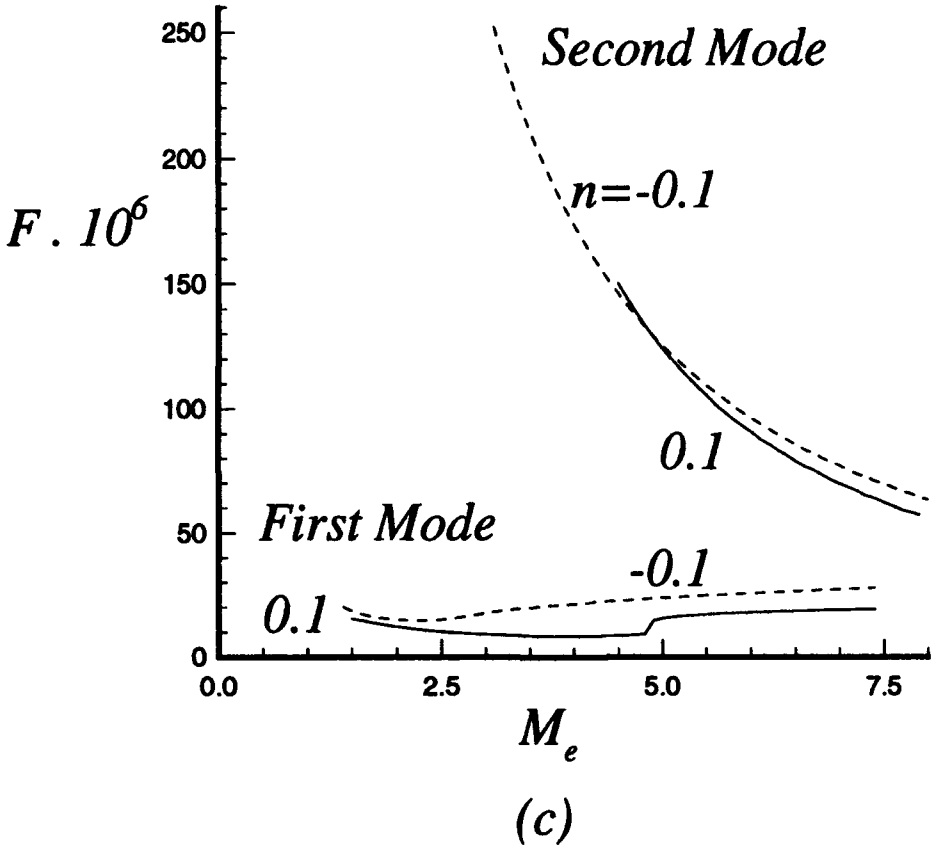

Figure 5. Continued.

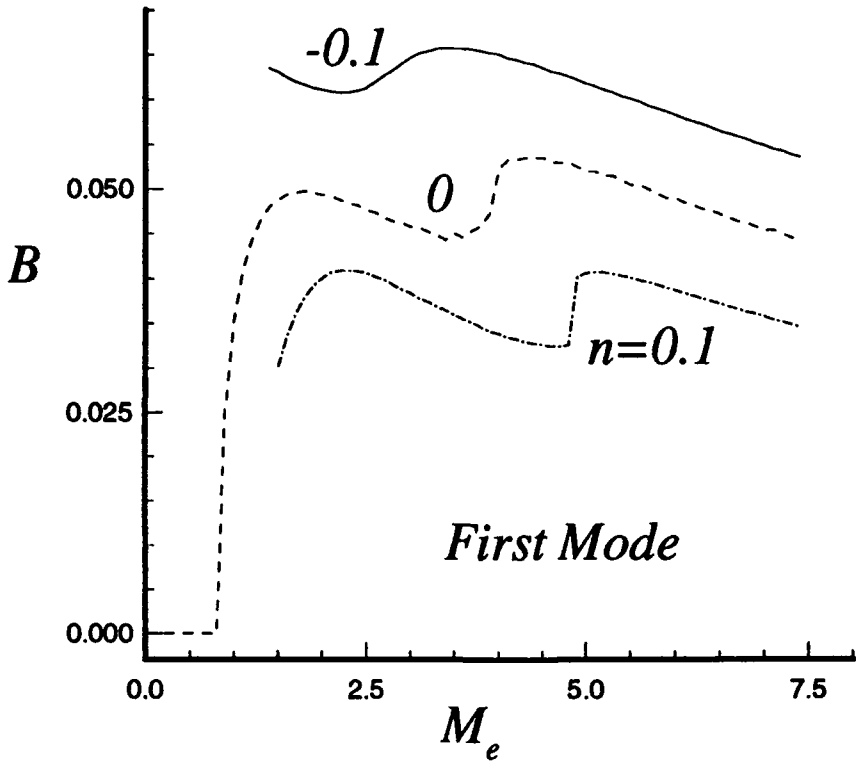

(d)

Figure 5. Concluded.

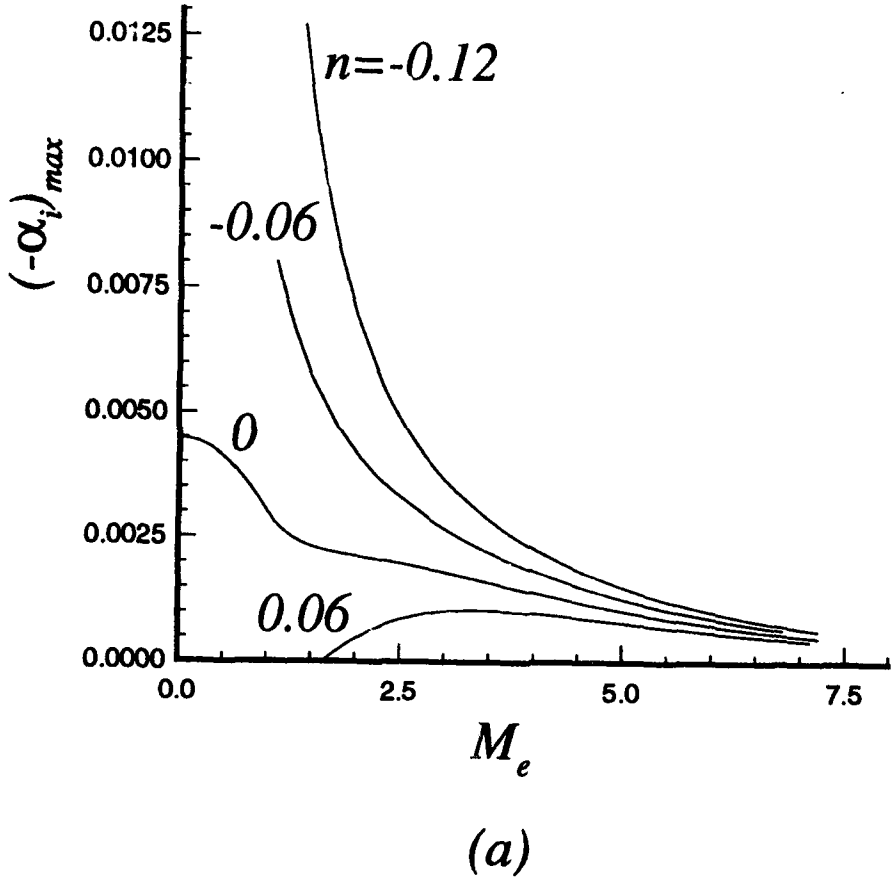

(a)

Figure 6. (a) Variation of maximum growth rate of 3-D first-mode waves with edge Mach number for several levels of pressure gradient at R = 600, Pr = 0.72, and T_∞ = 120 K; (b) Corresponding streamwise wave numbers; (c) Corresponding frequencies; and (d) Corresponding spanwise wave-number parameters.

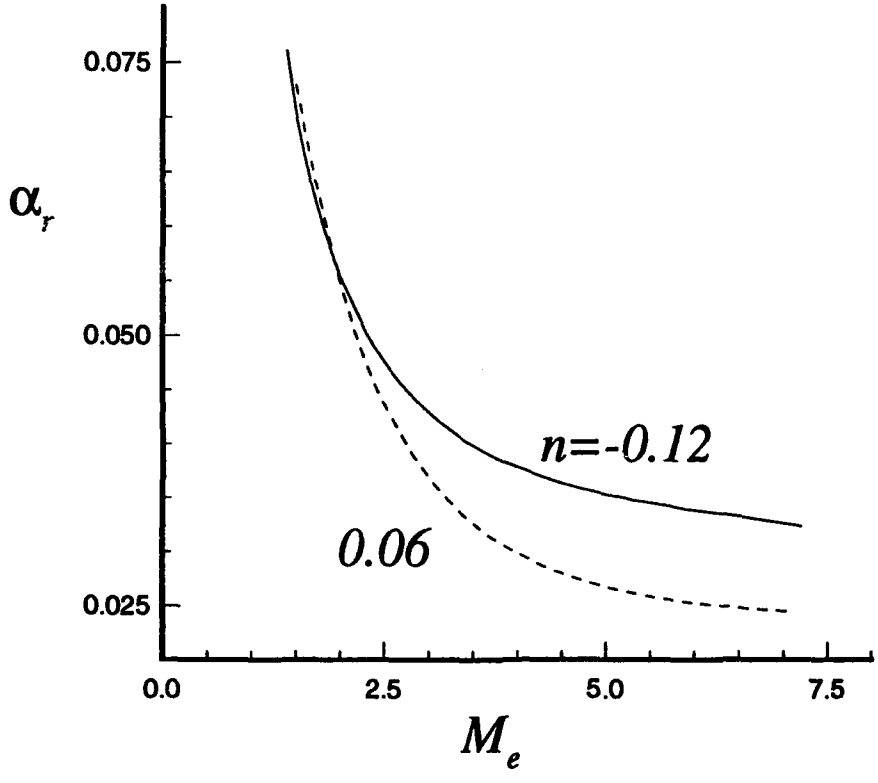

(b)

Figure 6. Continued.

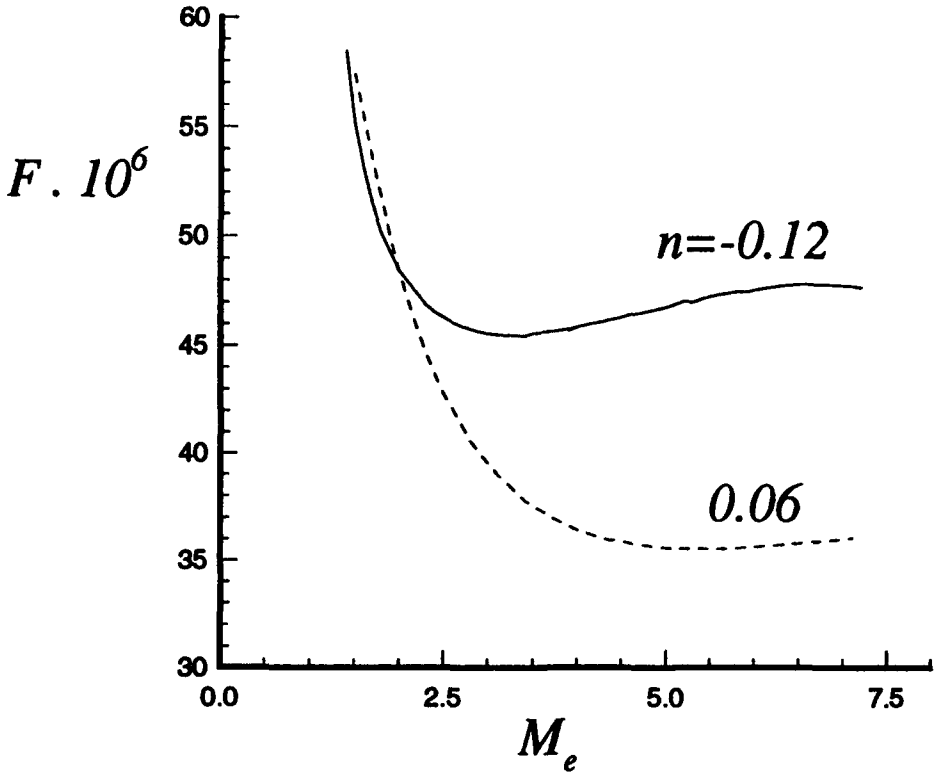

(c)

Figure 6. Continued.

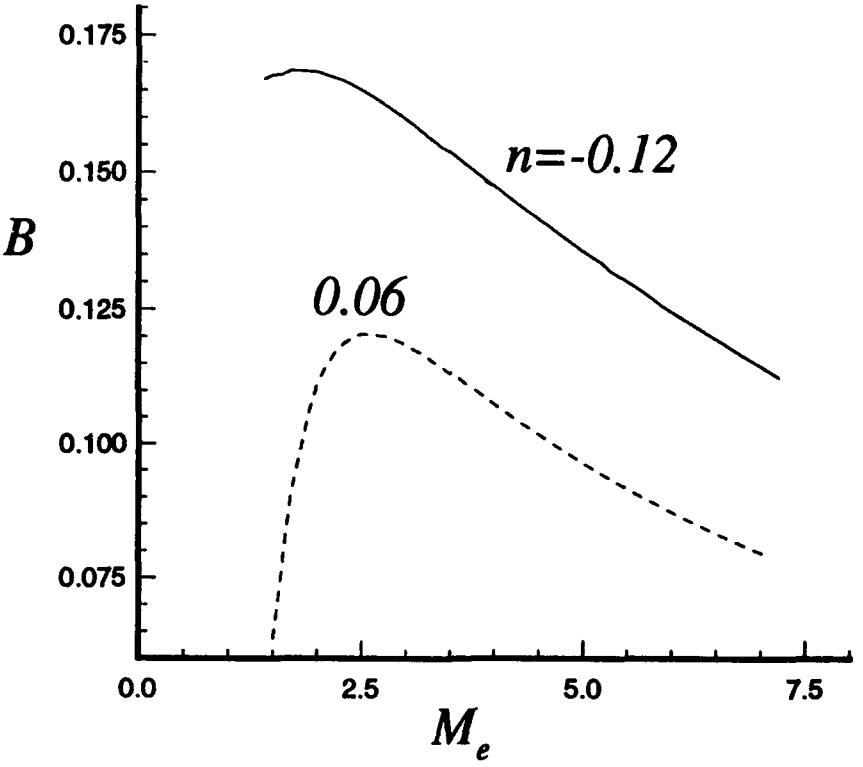

(d)

Figure 6. Concluded.

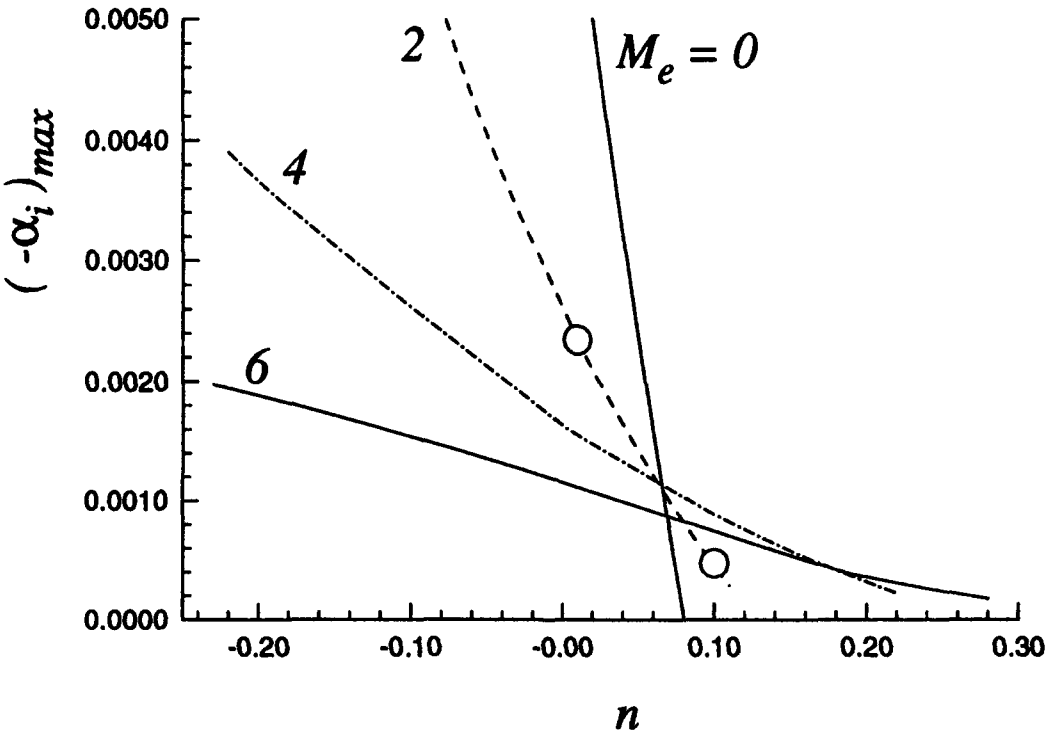

Figure 7. Variation of maximum growth rate of 3-D first-mode waves with pressure-gradient parameter for several edge Mach numbers at R = 1500, Pr = 0.72, and T_∞ = 120 K.

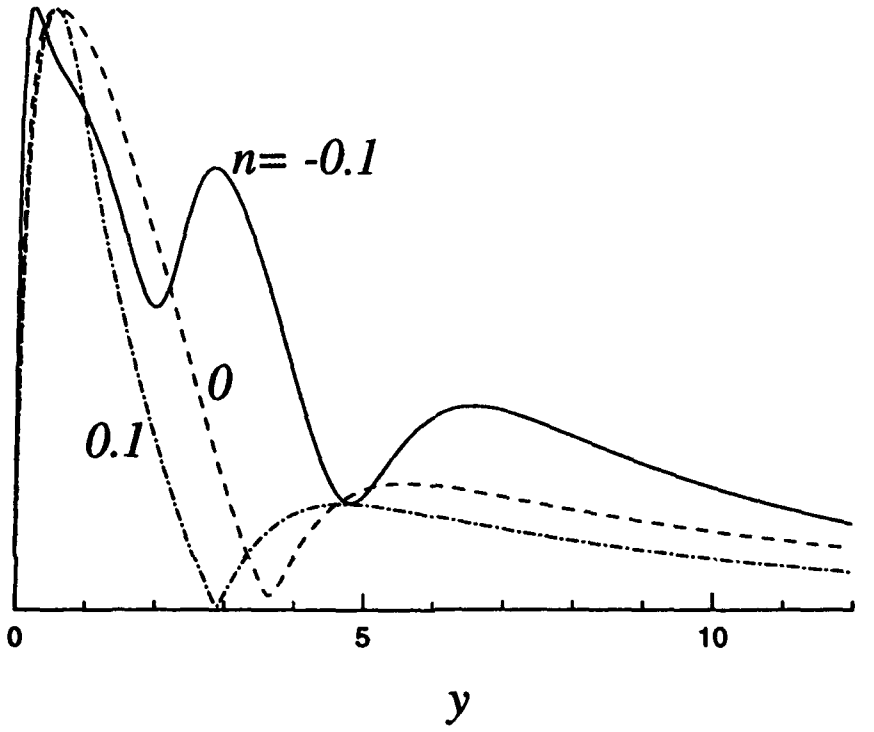

Figure 8. Transverse distribution of streamwise velocity fluctuations at $M_\infty = 0, R = 1500$, $Pr = 0.72$, and $T_\infty = 120$ K.

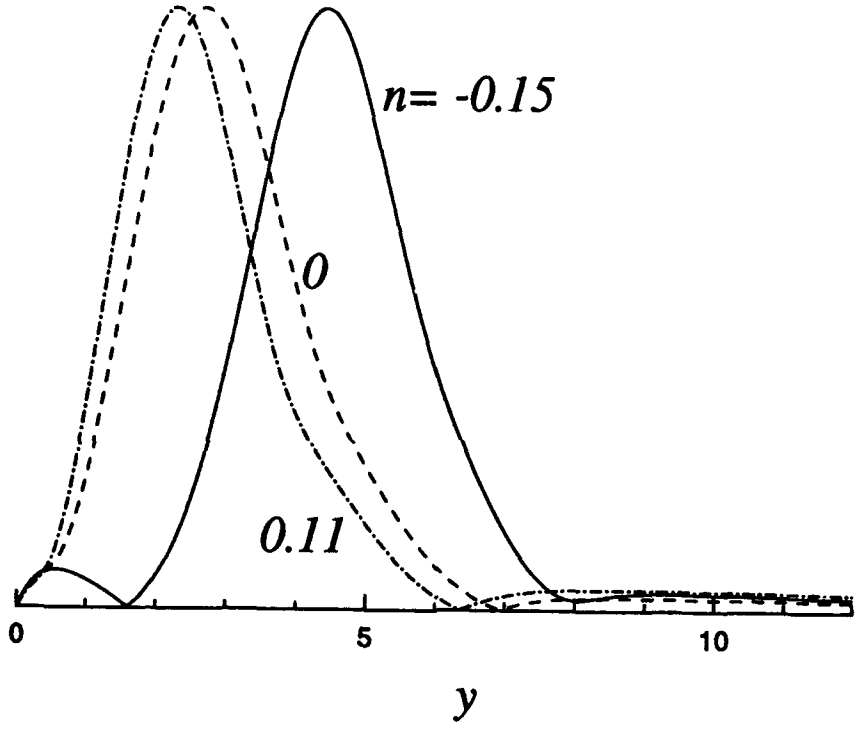

(a)

Figure 9. Transverse distribution of (a) streamwise velocity and (b) temperature fluctuations at $M_\infty = 2, R = 1500, Pr = 0.72$, and $T_\infty = 120$ K.

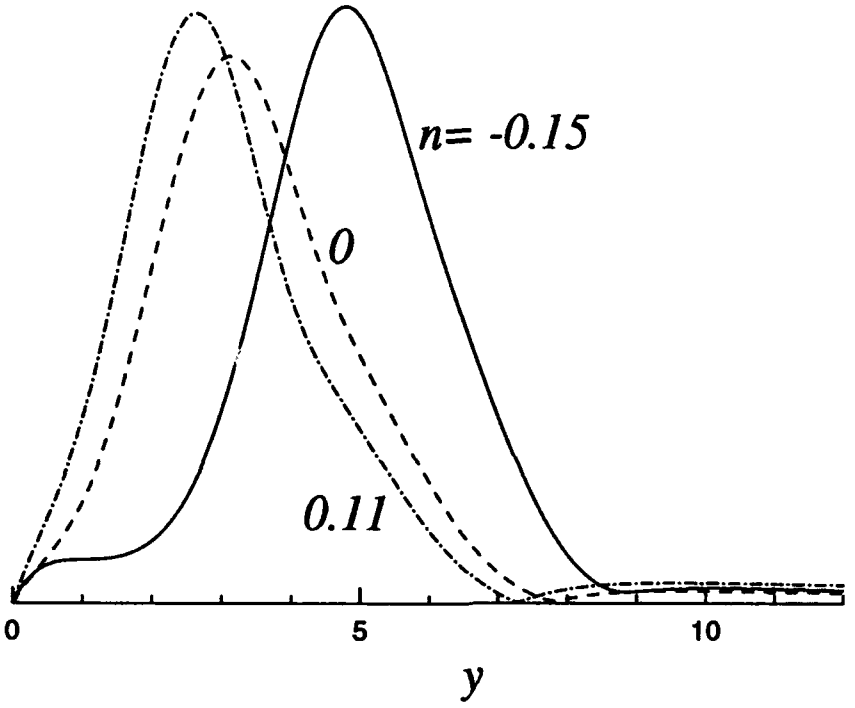

(b)

Figure 9. Concluded.

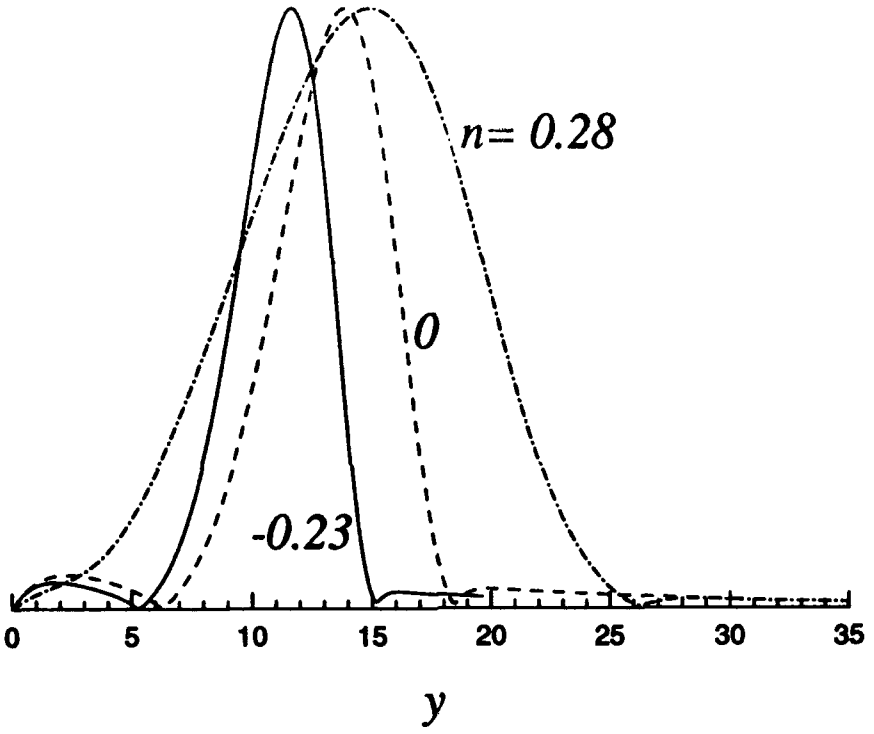

(a)

Figure 10. Transverse distribution of (a) streamwise velocity and (b) temperature fluctuations at $M_\infty = 6, R = 1500, Pr = 0.72$, and $T_\infty = 120$ K.

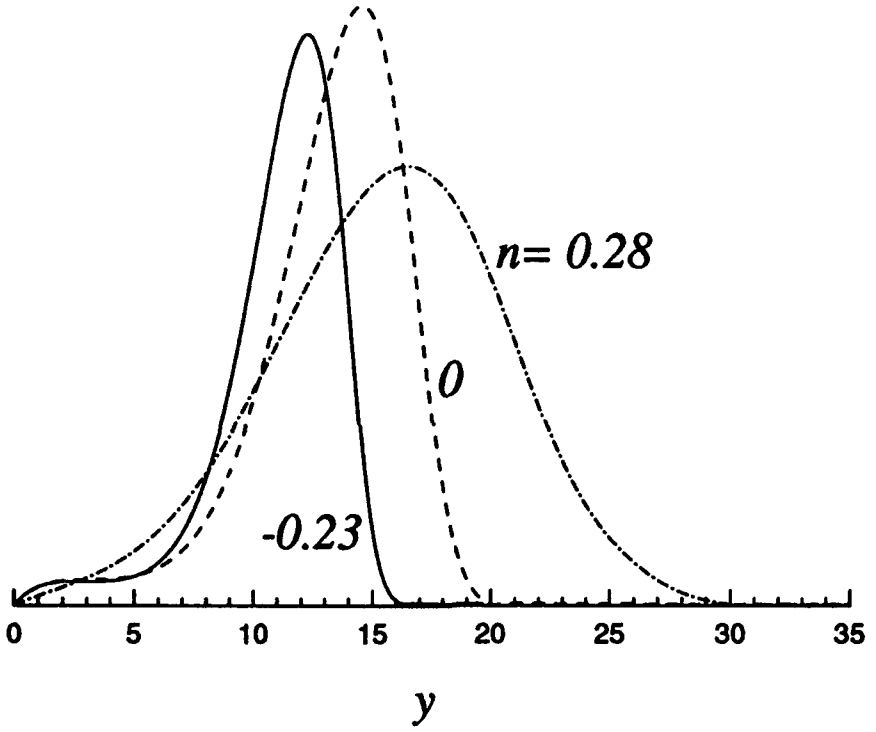

(b)

Figure 10. Concluded.

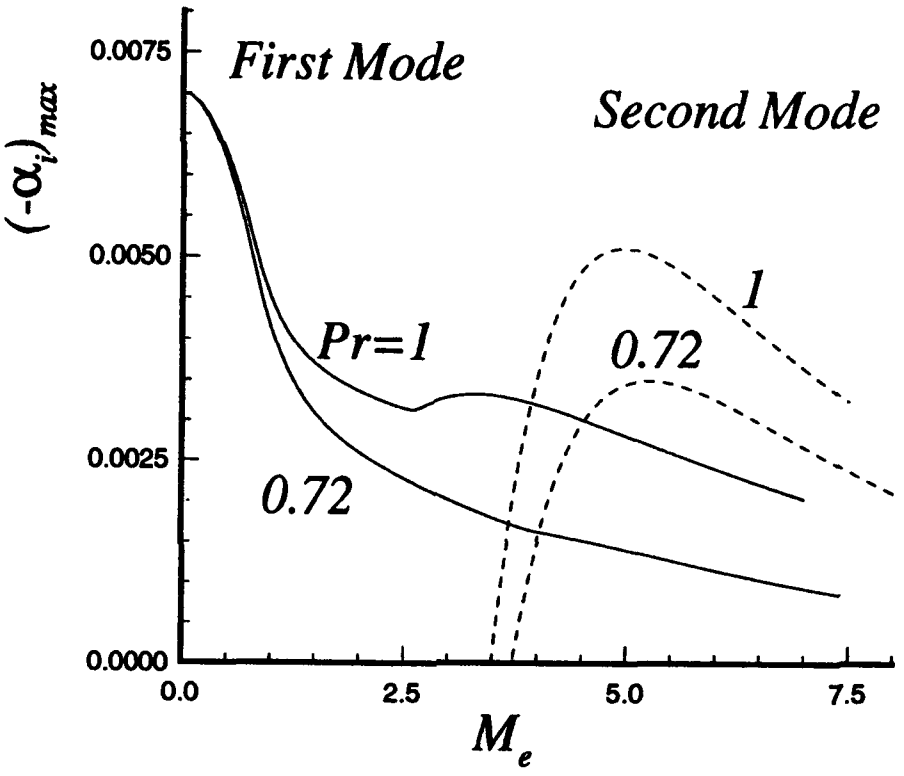

Figure 11. Variation of maximum growth rate with edge Mach number for two values of Prandtl number at R = 1500, T_∞ = 120 K, and zero pressure gradient.

REPORT DOCUMENTATION PAGE

Form Approved
OMB No. 0704-0188

1. AGENCY USE ONLY *(Leave blank)*	2. REPORT DATE	3. REPORT TYPE AND DATES COVERED
	April 1994	Contractor Report

4. TITLE AND SUBTITLE
EFFECT OF PRESSURE GRADIENT ON FIRST MODE OF INSTABILITY IN HIGH-SPEED BOUNDARY LAYERS

5. FUNDING NUMBERS
C NAS1-19480
WU 505-90-52-01

6. AUTHOR(S)
Jamal A. Masad
Yousef H. Zurigat

7. PERFORMING ORGANIZATION NAME(S) AND ADDRESS(ES)
Institute for Computer Applications in Science
and Engineering
Mail Stop 132C, NASA Langley Research Center
Hampton, VA 23681-0001

8. PERFORMING ORGANIZATION REPORT NUMBER
ICASE Report No. 94-31

9. SPONSORING/MONITORING AGENCY NAME(S) AND ADDRESS(ES)
National Aeronautics and Space Administration
Langley Research Center
Hampton, VA 23681-0001

10. SPONSORING/MONITORING AGENCY REPORT NUMBER
NASA CR-194910
ICASE Report No. 94-31

11. SUPPLEMENTARY NOTES
Langley Technical Monitor: Michael F. Card
Final Report
Submitted to Physics of Fluids

12a. DISTRIBUTION/AVAILABILITY STATEMENT
Unclassified–Unlimited

Subject Category 34

12b. DISTRIBUTION CODE

13. ABSTRACT *(Maximum 200 words)*
The effect of a pressure gradient on the first mode of instability of compressible subsonic and supersonic boundary layers is investigated using linear stability theory. Formulations are presented for nonsimilar boundary-layer mean flow and linear quasi-parallel stability problems that account for variable fluid properties. A pressure gradient is studied that generates potential-flow Mach number distributions at the edge of the boundary layer of the form $M_e = cx^n$, where c is a constant and x is the dimensionless streamwise distance. Variations are calculated for the maximum growth rates of three-dimensional first-mode waves with different edge Mach numbers and different levels of both adverse and favorable pressure gradients. A favorable pressure gradient is shown to have a stabilizing effect on first- mode waves. However, at high edge Mach numbers, a favorable pressure gradient becomes less effective in stabilizing first-mode waves. The frequencies and streamwise and spanwise wave numbers that correspond to the maximum growth rates of first-mode waves decrease as the pressure gradient become more favorable at all Mach numbers when the Reynolds number R = 1500 and at $M_e \geq 2$ when $R = 600$. Setting the Prandtl number to unity significantly increases the maximum growth rates of first- and second-mode waves at high Mach numbers compared with setting it to the realistic value of 0.72.

14. SUBJECT TERMS
Pressure gradient, stability,
supersonic, boundary layers

15. NUMBER OF PAGES
52

16. PRICE CODE
A04

17. SECURITY CLASSIFICATION OF REPORT	18. SECURITY CLASSIFICATION OF THIS PAGE	19. SECURITY CLASSIFICATION OF ABSTRACT	20. LIMITATION OF ABSTRACT
Unclassified	Unclassified		